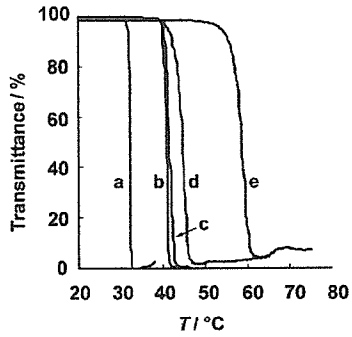

Figure 1. Effect of temperature on transmittance of a) PNIPAAm, b) poly(NIPAAm-*co*-AAm), c) NIPAM-0-G4.5, d) NIPAM-4-G5, and e) NIPAM-3-G5 dissolved in 10 mM phosphate solution (10 mg mL^{-1}, pH 9.0).

Similarly, solutions of NIPAM-terminated dendrimers showed a sharp decrease in turbidity at a certain temperature: the LCSTs for the solutions of NIPAM-0-G4.5, NIPAM-3-G5, and NIPAM-4-G5 dendrimers were estimated as 41, 56, and 43 °C, respectively. This result further confirms that the introduction of a common structural unit to the surface of dendrimers can impart temperature-sensitive properties to them.[4,7] Although these dendrimers have the same number of NIPAM groups on the periphery, they exhibit different LCSTs. As their molecular structures show (Scheme 1), the length of the spacer moiety between the tertiary amine at the outermost branching point and the terminal NIPAM group increases in the order of NIPAM-0-G4.5 < NIPAM-3-G5 < NIPAM-4-G5 dendrimers. The increase in spacer length might decrease the density of NIPAM groups in the dendrimer periphery. Such a situation could depress the occurrence of phase transition of the dendrimer.[4] However, the hydrophobicity of the spacer moiety might increase with increasing spacer length, which enhances the occurrence of the phase transition. These opposing effects of the spacer length could cause the deviation of the LCSTs of the dendrimers.

Next, we characterized the transitions of the NIPAM-bearing polymers and dendrimers by differential scanning calorimetry (DSC; Figure 2).[2,8] PNIPAAm and poly(NIPAAm-*co*-AAm) showed endothermic peaks centered at 31.4

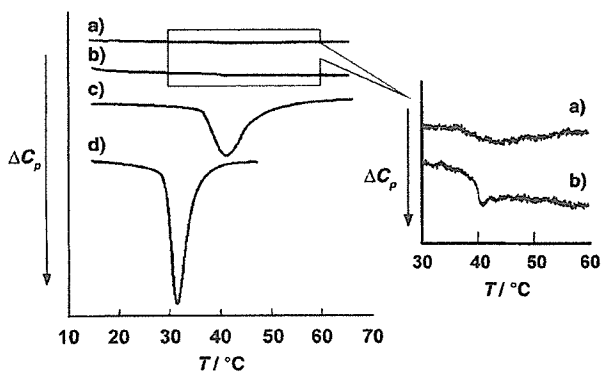

Figure 2. DSC thermograms of a) NIPAM-0-G4.5, b) NIPAM-4-G5, c) poly(NIPAAm-*co*-AAm), and d) PNIPAAm. The heating rate was 0.5 K min^{-1}. C_p = heat capacity.

and 41.0 °C, respectively, which agree with their LCSTs (Figure 1). Similarly, the NIPAM-terminated dendrimers exhibited an endothermic peak around the LCST. However, a striking difference is apparent between the DSC curves for the NIPAM-terminated dendrimers and the linear polymers: the heat of transition for the former is extremely small.

The cloud points and transition enthalpies (ΔH) for these thermosensitive polymers and dendrimers are summarized in Table 1. The phase separation or precipitation of thermosensitive polymers has been explained from the viewpoint of entropy effects in the polymer solution.[2,9] At low temperatures, strong hydrogen bonding between hydrophilic amide groups and water exceeds the unfavorable free energy related to the exposure of hydrophobic isopropyl groups to water. With increasing temperature, hydrophobic interaction between isopropyl groups is enhanced, whereas hydrogen bonding is weakened. Therefore, at temperatures higher than the LCST, interaction between hydrophobic groups becomes dominant, thereby resulting in the entropy-driven polymer collapse and concomitant release of structured water around the hydrophobic groups, which requires the absorption of heat.[2,9]

Table 1: Transition enthalpies of various thermosensitive polymers.

Polymer	Cloud point [°C]	T_{max} [°C][a]	ΔH [J g^{-1}]	ΔH [kJ mol^{-1} of NIPAM unit]
PNIPAAm	32.2	31.4	34.3	3.88
poly(NIPAAmM-*co*-AAm)	40.2	41.0	21.1	2.79
NIPAM-0-G4.5	40.6	43.8	0.3	0.07
NIPAM-4-G5	43.2	40.4	0.2	0.08

[a] Evaluated by DSC.

As shown in Table 1, the transition enthalpy of poly(NIPAAm-*co*-AAm) is somewhat lower than that of PNIPAAm because hydration of hydrophobic groups decreases with increasing temperature.[9] However, compared to these linear polymers, the dendrimers exhibit transition enthalpies that are two orders of magnitude lower, even though these polymers and dendrimers include the same hydrophobic groups. Indeed, the weight percent of NIPAM groups in the whole molecule differs among these polymers and dendrimers. Consequently, the transition enthalpy is normalized by the number of NIPAM groups in a molecule, but much smaller values are still apparent for the dendrimers after the normalization compared with those of the linear polymers (Table 1).

The release of the structured water might take place not only from NIPAM groups, but also from the polymer backbone for the linear polymers. However, a larger fraction of hydrophobic carbon atoms exists in the NIPAM groups. These side groups play a crucial role in the thermosensitive properties of the polymers. Therefore, hydration or dehydration of NIPAM groups before and after the transition might be responsible for the large difference between the transition enthalpies of the linear polymers and globular dendrimers.

The dendrimer surface should exhibit a more hydrophobic nature if NIPAM groups in the periphery of the dendrimer are

less hydrated than the NIPAM-bearing linear polymers. Therefore, we examined the hydrophobicity of these NIPAM-bearing polymers below the LCST using 1-pyrenecarboxaldehyde (PyCHO), which changes the wavelength of the emission maximum (λ_{max}) depending on the polarity of the solvent.[10,11]

Figure 3 shows the dependence of λ_{max} on the concentration of NIPAM-terminated dendrimers, PNIPAAm, and poly(NIPAAm-*co*-AAm) below the LCST. The result for the

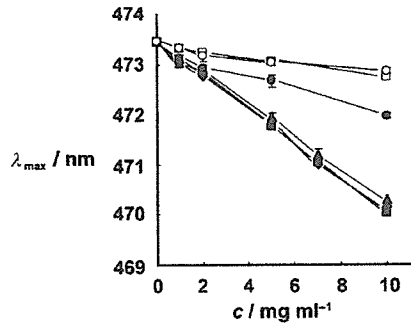

Figure 3. Emission maxima of PyCHO (1 μM) as a function of the concentration of NIPAM-0-G4.5 (■), NIPAM-3-G5 (▲), NIPAM-4-G5 (◆), OH-terminated G5 (●), PNIPAAm (□), and poly(NIPAAmM-*co*-AAm) (○) dissolved in 10 mM phosphate solution (pH 9.0) at 20 °C. λ_{ex} = 365.5 nm.

OH-terminated PAMAM G5 dendrimer is also given, as a dendrimer without NIPAM groups in the periphery. The presence of PNIPAAm or poly(NIPAAm-*co*-AAm) only slightly affected λ_{max} even at a high concentration of 10 mg mL^{-1}, which indicates that these linear polymers do not form domains with a hydrophobic nature. However, in the presence of NIPAM-terminated dendrimers, a blue shift of λ_{max} was observed with increasing concentration of the dendrimers. The OH-terminated PAMAM-G5 dendrimer caused a blue shift of λ_{max} which was much less than that caused by NIPAM-terminated dendrimers. These dendrimers contain the same interior. Therefore, the marked change of λ_{max} in the presence of the NIPAM-terminated dendrimers might be attributable to the peripheral NIPAM groups. Probably, the dense packing of NIPAM groups in the dendrimer periphery enhances dehydration around these groups.

To confirm the low extent of hydration of the dendrimer NIPAM groups, we further investigated the influence of urea on the LCST, because urea is known to modify hydration around hydrophobic solutes in aqueous solutions and to reduce hydrophobic interactions.[12] The presence of urea did not affect the LCST of the PNIPAAm solution (Figure 4a). Fang et al. reported that the presence of urea at a concentration of 3 M did not change the LCST of PNIPAAm, although swelling of the compact conformation of the polymer chain was caused by urea at temperatures higher than the LCST.[13] In contrast, a marked difference is apparent for the NIPAM-terminated dendrimer, which exhibited a considerable increase of LCST with increasing urea concentration.

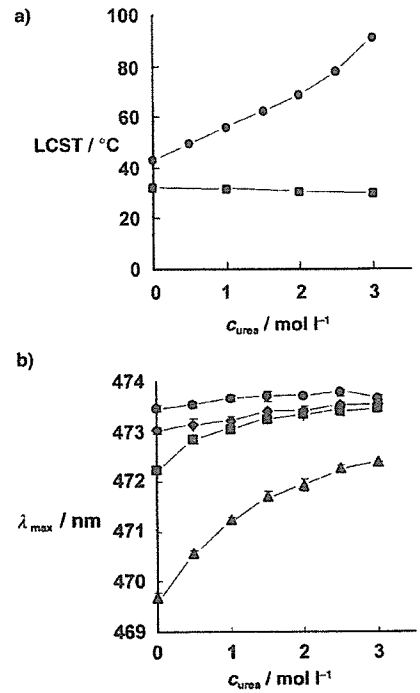

Figure 4. a) Influence of urea on LCST of NIPAM-4-G5 (●) and PNIPAAm (■) dissolved in 10 mM phosphate solution (10 mg mL^{-1}, pH 9.0). b) Influence of urea on emission maxima of PyCHO (1 μM) in 10 mM phosphate solution in the absence (●) or presence (◆) of PNIPAAm, PAMAM-OH G5 (■), and NIPAM-4-G5 (▲) at 20 °C.

The effects of urea on the hydrophobicity of the NIPAM-bearing dendrimer and linear polymers were also examined using PyCHO (Figure 4b). Although the effects on PNIPAAm and OH-terminated PAMAM G5 dendrimer were negligible, the NIPAM-terminated dendrimer displayed a considerable increase in λ_{max} with increasing urea concentration. Probably, urea molecules disturb the hydrophobic interaction of NIPAM groups and reduce their dehydration in the surface of the dendrimer.

The different hydration states around NIPAM groups that arise from the structural features of these linear and globular polymers are illustrated schematically in Figure 5. For NIPAM-bearing linear polymers, their backbone has a large conformational freedom, which enables efficient hydration of NIPAM groups below the LCST and efficient association of NIPAM groups above the LCST. For that reason, a large

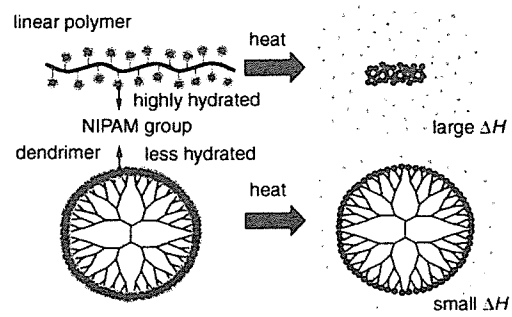

Figure 5. Schematic illustration of the phase transition of NIPAM-bearing polymer with a globular or a linear structure.

amount of structured water that solvates around NIPAM groups can be released upon the transition, thus yielding a large transition enthalpy. However, for the NIPAM-terminated dendrimers, the low conformational freedom that arises from their highly branched structure might cause dense packing of NIPAM groups in the periphery. Such a situation should lead to inefficient hydration around NIPAM groups below the LCST and inefficient dehydration of the NIPAM groups above the LCST, thereby resulting in the extremely small transition enthalpy.

In conclusion, we have demonstrated that marked differences exist in transition enthalpy, hydrophobicity, and sensitivity to urea between NIPAM-bearing dendrimers and linear polymers, which arise from their structural features. The thermosensitive dendrimers could undergo a sharp transition by dehydration of the peripheral moiety without a large conformational change of the whole molecule. Such properties, as well as the globular shape of the thermosensitive dendrimers, might be attractive for their use as intelligent nanocapsules for drug delivery and catalysis. The findings obtained through this study increase the understanding of thermosensitive polymers and expand their range of application.

Received: August 16, 2006
Revised: October 4, 2006
Published online: November 24, 2006

Keywords: dendrimers · isopropylacrylamide · lower critical solution temperature · polymers · thermodynamics

[1] a) R. Yoshida, K. Uchida, Y. Kaneko, K. Sakai, A. Kikuchi, Y. Sakurai, T. Okano, *Nature* **1995**, *374*, 240–242; b) P. S. Stayton, T. Shimoboji, C. Long, A. Chilkoti, G. Chen, J. H. Harris, A. S. Hoffman, *Nature* **1995**, *378*, 472–474; c) K. Kono, *Adv. Drug Delivery Rev.* **2001**, *53*, 307–319; d) K. Nishida, M. Yamato, Y. Hayashida, K. Watanabe, K. Yamamoto, E. Adachi, S. Nagai, A. Kikuchi, N. Maeda, H. Watanabe, T. Okano, Y. Tano, *N. Engl. J. Med.* **2004**, *351*, 1187–1196; e) A. S. Hoffman, *Clin. Chem.* **2000**, *46*, 1478–1486.

[2] M. Heskins, J. E. Guillet, *J. Macromol. Sci. Chem. A* **1968**, *2*, 1441–1455.

[3] H. G. Schild, *Prog. Polym. Sci.* **1992**, *17*, 163–249.

[4] Y. Haba, A. Harada, T. Takagishi, K. Kono, *J. Am. Chem. Soc.* **2004**, *126*, 1276–12761.

[5] a) K. L. Wooley, J. M. Fréchet, C. J. Hawker, *Polymer* **1994**, *35*, 4489–4495; b) T. H. Mourey, S. R. Turner, M. Rubinstein, J. M. J. Fréchet, *Macromolecules* **1992**, *25*, 2401–2406; c) R. Haag, J. F. Staubé, A. Sunder, H. Frey, A. Hebel, *Macromolecules* **2000**, *33*, 8158–8166.

[6] a) C. Kojima, Y. Haba, K. Kono, T. Takagishi, *Macromolecules* **2003**, *36*, 2183–2186; b) Y. Haba, A. Harada, T. Takagishi, K. Kono, *Polymer* **2005**, *46*, 1813–1820.

[7] Y. Haba, C. Kojima, A. Harada, K. Kono, *Macromolecules* **2006**, *39*, 7451–7453.

[8] a) L. D. Taylor, L. D. Cerankowski, *J. Polym. Sci. Polym. Chem. Ed.* **1975**, *13*, 2551–2570; b) H. G. Schild, D. A. Tirrell, *J. Phys. Chem.* **1990**, *94*, 4352–4356; c) E. I. Tiktopulo, V. E. Bychkova, J. Ricka, O. B. Ptitsyn, *Macromolecules* **1994**, *27*, 2879–2882.

[9] H. Feil, Y. H. Bae, J. Feijen, S. W. Kim, *Macromolecules* **1993**, *26*, 2496–2500.

[10] K. Kalyanasundaran, J. K. Thomas, *J. Phys. Chem.* **1977**, *81*, 2176–2180.

[11] H. G. Schild, D. A. Tirrell, *Langmuir* **1991**, *7*, 1319–1324.

[12] a) W. Bruning, A. Holtzer, *J. Am. Chem. Soc.* **1961**, *83*, 4865–4866; b) R. A. Kuharski, P. J. Rossky, *J. Am. Chem. Soc.* **1984**, *106*, 5794–5800.

[13] Y. Fang, J. C. Qiang, D. D. Hu, M. Z. Wang, Y. L. Cui, *Colloid Polym. Sci.* **2001**, *279*, 14–21.

Control of Temperature-Sensitive Properties of Poly(amidoamine) Dendrimers Using Peripheral Modification with Various Alkylamide Groups

Yasuhiro Haba, Chie Kojima, Atsushi Harada, and Kenji Kono*

Department of Applied Chemistry, Graduate School of Engineering, Osaka Prefecture University, 1-1 Gakuen-cho, Nakaku, Sakai, Osaka 599-8531, Japan

Received May 6, 2006
Revised Manuscript Received August 7, 2006

Introduction

Dendrimers have various features that conventional linear polymers do not have.[1] Their size, structure, and surface properties are highly controllable. In addition, their interiors can encapsulate small molecules. Using these features of dendrimers, materials with unique and important functions are expected to be produced. Stimuli-sensitive properties are useful functions considering application of dendrimers in the fields of drug delivery[2] and catalysis.[3] Therefore, many efforts have been made to develop dendrimers with sensitivity to light[4] and oxdative−reductive environments.[5]

Regarding the preparation of dendrimers with temperature sensitivity, attempts have been made to graft poly(*N*-isopropylacrylamide) (PNIPAM), which is a well-known thermosensitive polymer with a lower critical solution temperature (LCST) of 32 °C, to chain ends of dendrimers.[6,7] Indeed, attachment of PNIPAM chains to the dendrimer surface produces dendrimers with temperature-sensitive shells. However, it is noteworthy that these PNIPAM-modified dendrimers lose their important characteristic of molecular uniformity because PNIPAM chains are fundamentally polydispersed. In addition, the molecular shape of the PNIPAM-modified dendrimers might more closely resemble that of star polymers rather than globular dendrimers.

Recently, we presented another strategy for preparation of thermosensitive dendrimers. We introduced isobutyramide (IBAM) group, a common structural unit with thermosensitive poly(*N*-vinylisobutyramide), to every chain end of dendrimers.[8] We observed that the IBAM-terminated poly(amidoamine) or poly(propylenimine) dendrimer exhibited lower critical solution temperature. This strategy is attractive because the resultant dendrimers with temperature-sensitive properties retain their globular structure and uniformity at the molecular level.

On the basis of this design of IBAM-modified dendrimers, a question of whether temperature-sensitive dendrimers are obtainable using surface modification with structural units common with thermosensitive polymers naturally arises. To address this question, we prepared PAMAM dendrimers in this study that have various alkylamide groups, which share structural similarity with thermosensitive polymers with linear structure.[9,10] The correlation between the structures of alkylamide groups in the dendrimer periphery and their temperature-sensitive properties has been described.

Results and Discussion

Previous studies have shown that various molecules that have a carboxyl group, such as isobutyric acid and *tert*-butyloxycarbonyl-protected amino acids, can be combined to every chain end of amine-terminated PAMAM dendrimers using the condensing agent 1,3-dicyclohexylcarbodiimide (DCC).[5,8,11] Therefore, in the same manner, we prepared PAMAM G4 dendrimers that have *n*-butyramide (NBAM), IBAM, and cyclopropanecarboxylic acid amide (CPCAM) groups at chain ends, which are designated as NBAM-G4, IBAM-G4, and CPCAM-G4, by the reaction of amine-terminated PAMAM G4 dendrimer with *n*-butyric acid, isobutyric acid, and cyclopropanecarboxylic acid using DCC (Scheme 1). Furthermore, PAMAM G5 dendrimers that have propionamide (PAM), NBAM, and *n*-valeramide (VAM) groups at chain ends, which are designated as PAM-G5, NBAM-G5, and VAM-G5, were synthesized using the reaction of amine-terminated PAMAM G5 dendrimer with the corresponding carboxylic acids in the same way. The numbers of alkylamide groups of the alkylamide-terminated dendrimers were evaluated using ^{1}H NMR (Table l). As shown in Table 1, the numbers of terminal alkylamide groups agree well with the numbers of the chain ends of the corresponding dendrimers for all alkylamide-modified dendrimers, indicating that essentially every chain end of the dendrimer is combined to the alkylamide group for these modified dendrimers.

First, we investigated the influence of the length of the terminal alkylamide groups on thermosensitivity of the alkylamide-terminated dendrimers. Figure 1 portrays the temperature dependence of the light transmittance of PAM-G5, NBAM-G5, and VAM-G5 dissolved in 10 mM phosphate solution of pH 9.0 at 500 nm. The solution of the PAM-G5 dendrimer was transparent over the experimental temperature range. However, the solutions of NBAM-G5 and VAM-G5 dendrimers became turbid at 43 and 11 °C, respectively, indicating that these dendrimer solutions underwent phase separation at these temperatures. In general, the LCST of thermosensitive polymers is known to decrease with increasing hydrophobicity of the polymer chains.[9,10,12] Regarding poly(*N*-vinylalkylamide)s, which are polymers with a linear structure that shares common structural units with these alkylamide-terminated dendrimers, the LCST of poly(*N*-vinyl-*n*-butyramide) is reported as 32 °C. In contrast, poly(*N*-vinyl-*n*-valeramide) is insoluble in water, even in cold water, because of its hydrophobic side groups.[9] Therefore, it is likely that PAM groups are too hydrophilic to provide thermosensitive properties to the PAMAM G5 dendrimer, whereas NBAM and VAM groups might have appropriate hydrophobicity to yield dendrimer with temperature sensitivity.

Next, for alkylamide-terminated dendrimers, we investigated the influence of structures of terminal alkylamide groups that have the same number of carbon atoms on their thermosensitive properties. Figure 2 shows the temperature dependence of the light transmittance of NBAM-G4, IBAM-G4, and CPCAM-G4 dissolved in 10 mM phosphate solution of pH 9.0 at 500 nm. Solutions of NBAM-G4, IBAM-G4, and CPCAM-G4 exhibited the cloud points at 45, 61, and 15 °C, respectively.

Hydrophobicity of alkyl group with a branch or cyclic structure is known to be lower than for the alkyl group of the same number of carbon atoms with a linear structure. We calculated logarithms of 1-octanol−water partition coefficient (log *P*), which are used to estimate hydrophobicity of a molecule, for *N*-ethylbutyramide, *N*-ethylisobutyramide, and cyclopropanecarboxylic acid ethylamide, which bear structural similarity to the terminal moiety of the alkylamide-modified

* Corresponding author: Tel and Fax: +81-72-254-9330; e-mail: kono@chem.osakafu-u.ac.jp.

10.1021/ma061019a CCC: $33.50
Published on Web 09/07/2006

Scheme 1. Synthesis of PAMAM G4 and G5 Dendrimers Having Various Alkylamide Groups at Chain Ends

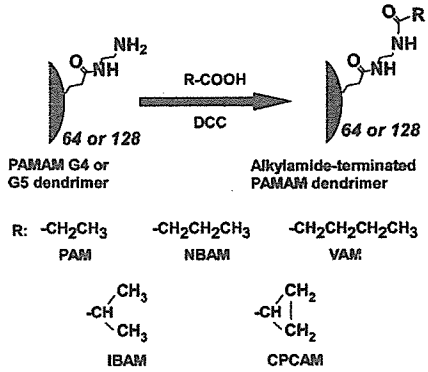

Table 1. Characterization of Various Alkylamide-Terminated Dendrimers[a]

dendrimer	no. of chain ends	no. of terminal alkylamide groups incorporated
PAM-G5	128	130.5
NBAM-G5	128	131.5
VAM-G5	128	130.3
NBAM-G4	64	64.5
IBAM-G4	64	64.2
CPCAM-G4	64	63.8

[a] Determined by ^{1}H NMR.

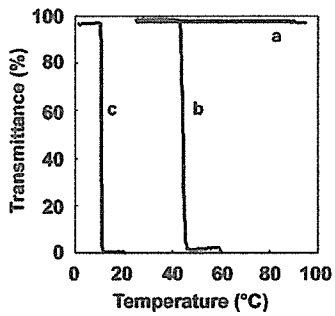

Figure 1. Effect of temperature on transmittance of PAM-G5 (a), NBAM-G5 (b), and VAM-G5 (c) dissolved in 10 mM phosphate solution (10 mg/mL, pH 9.0).

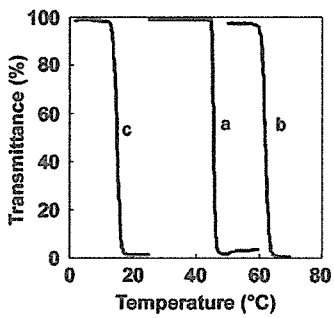

Figure 2. Effect of temperature on transmittance of (a) IBAM-G4, (b) NBAM-G4, and (c) CPCAM-G4 dissolved in 10 mM phosphate solution (10 mg/mL, pH 9.0).

dendrimer, as 0.84, 0.59, and 0.24, respectively, using Broto's fragmentation method.[13] Therefore, the hydrophobicity of peripheral alkylamide groups is inferred to increase in the order of CPCAM-G4 < IBAM-G4 < NBAM-G4. In fact, Ito reported that LCSTs of poly(*N*-cyclopropylacrylamide), poly(*N*-isopropylacrylamide), and poly(*N*-*n*-propylacrylamide) decreased with the same order, suggesting that hydrophobicity of the alkylamide groups can determine LCST for these polymers.[10]

However, in the case of the alkylamide-terminated dendrimers, their LCST is not simply determined by hydrophobicity of

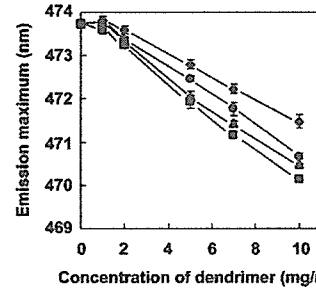

Figure 3. Emission maxima for PyCHO in aqueous solutions of hydroxyl-terminated PAMAM-G4 (diamonds), IBAM-G4 (circles), NBAM-G4 (triangles), and CPCAM-G4 (squares) at 4 °C.

the terminal alkylamide groups because CPCAM-G4 dendrimer showed the lowest cloud point temperature among these modified G4 dendrimers. Considering that conformational freedom of CPCAM groups is much lower than that of IBAM or NBAM groups, CPCAM groups might be highly concentrated in the peripheral region of the dendrimer.

We examined NMR relaxation times (T_1) for the terminal alkylamide groups attached to the dendrimers to obtain information on their mobility. The T_1 values for the terminal methyl/methylene protons of NBAM, IBAM, and CPCAM groups in the periphery of the dendrimers were evaluated to be 1.366, 0.882, and 0.682 s, respectively, whereas those for the same protons of the corresponding carboxylic acids used for the preparation of these alkylamide-terminated dendrimers were 2.973, 2.331, and 2.569 s, respectively. This result indicates that the CPCAM groups are most tightly packed in the dendrimer periphery and have the lowest mobility among these terminal groups. Therefore, it is likely that the dendrimer periphery crowded with CPCAM groups can enable their efficient interaction, resulting in the phase separation at the lowest temperature.

We further examined hydrophobicity of these alkylamide-terminated PAMAM G4 dendrimers using 1-pyrenecarboxaldehyde (PyCHO) to obtain insight into the low phase separation temperature of the CPCAM-G4 dendrimer. This molecule is known to change emission maxima (λ_{max}) depending on polarity of the solvent.[14] As shown in Figure 3, PyCHO displayed a more marked blue shift of λ_{max} in the presence of alkylamide-terminated dendrimers than in the case of hydroxyl-terminated G4 dendrimer. These dendrimers possess the same interior. Therefore, the large blue shift of the alkylamide-terminated dendrimers might indicate higher hydrophobicity of the peripheral region of these dendrimers. In addition, the CPCAM-G4 dendrimer exhibits a slightly larger blue shift, which is indicative of the slightly higher hydrophobic nature of this dendrimer's surface. As already mentioned, the log *P* values for these alkylamide groups indicate that CPCAM group has the lowest hydrophobicity among these alkylamide groups. However, CPCAM groups are most densely packed in the dendrimer periphery among them. Probably, the dense packing of the CPCAM groups in the dendrimer periphery might reduce contact with water molecules efficiently and form the hydrophobic surface.

From a practical viewpoint, control of LCST of thermosensitive dendrimers is very important. For thermosensitive polymers with a linear structure, copolymerization with monomers having appropriate hydrophilicity or hydrophobicity is widely used to control LCST.[9,12,15] Therefore, finally, we examined controllability of LCST of the dendrimer by adjusting the ratio of peripheral alkylamide groups. Three kinds of PAMAM G4 dendrimer having IBAM and CPCAM groups of 15 and 49, 29

Table 2. Preparation of IBAM-CPCAM-G4 Dendrimers[a]

dendrimer	in feed (mol %)		obtained (mol %)	
	isobutyric acid	cyclopropanecarboxylic acid	IBAM	CPCAM
IBAM-CPCAM(1/3)-G4	25	75	23.5	76.5
IBAM-CPCAM(1/1)-G4	50	50	45.9	54.1
IBAM-CPCAM(3/1)-G4	75	25	70.3	29.7

[a] Determined by ^{1}H NMR.

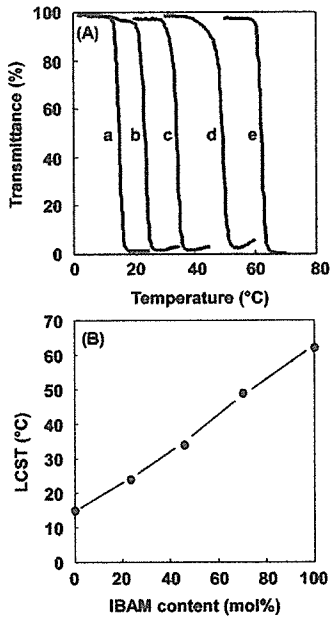

Figure 4. Influence of the IBAM/CPCAM ratio in the periphery on cloud point of IBAM-CPCAM-G4 dendrimers. (A) Effect of temperature on transmittance of dendrimers with IBAM/CPCAM (mol/mol) ratios of (a) 0/1, (b) 1/3, (c) 1/1, (d) 3/1, and (e) 1/0. The dendrimers were dissolved in 10 mM phosphate solution (10 mg/mL, pH 9.0). (B) Cloud point of IBAM-CPCAM-G4 dendrimers as a function of the content of IBAM groups (mol %) in the peripheral alkylamide groups.

and 35, and 45 and 19 per dendrimer were prepared with the PAMAM G4 dendrimer by adjusting the ratio of the corresponding carboxylic acids during their condensation (Table 2). Figure 4A depicts the temperature dependence of transmittance of the dendrimers that have IBAM and CPCAM groups at varying ratios. These dendrimers exhibited change in transmittance at different temperatures, indicating that their cloud point is dependent on the ratio of IBAM/CPCAM in the periphery. Despite the large difference of temperature regions of their cloud points, these dendrimers showed a sharp change in water solubility. Figure 4B represents the cloud points of the dendrimers with IBAM and CPCAM groups as a function of the percentage of IBAM groups in the terminal alkylamide groups. Apparently, the cloud point of the dendrimer increased with increasing IBAM fraction. This result indicates that dendrimers that exhibit a response at a desired temperature are obtainable by controlling the relative composition of terminal alkylamide groups.

As shown in this study, surface modification with alkylamide groups that are common structural units with well-known thermosensitive polymers with a linear structure provides temperature-sensitive properties to PAMAM dendrimers. Previously, we demonstrated that modification with IBAM groups, which is a structural unit of thermosensitive polymer poly(*N*-vinylisobutyramide), can provide temperature-sensitive properties to PAMAM dendrimers.[8] Through this study, we further generalized this strategy for production of thermosensitive dendrimers.

Dendrimers that exhibit LCST are thermosensitive polymers with highly unique features, such as having a three-dimensional structure and being monodispersed. In addition, dendrimers that exhibit thermosensitive properties in aqueous solutions are of importance from the practical standpoint. For example, dendrimers with LCST around physiological temperature could be used for site-specific drug delivery because such dendrimers could release drug and/or control interaction with cells at the target site heated. Only few dendrimers have been reported to exhibit temperature-sensitive properties so far.[8,16,17] Therefore, findings obtained in this study provide an efficient method to produce thermosensitive dendrimers and lead to a generation of a new family of thermosensitive polymers.

Acknowledgment. The authors thank Dr. Yagi, Osaka Prefecture University, for his support in NMR measurements. This research was partly supported by the Sasakawa Scientific Research Grant from The Japan Science Society.

Supporting Information Available: Experimental procedures. This material is available free of charge via the Internet at http://pubs.acs.org

References and Notes

(1) Tomalia, D. A.; Fréchet, J. M. J. *J. Polym. Sci., Part A: Polym. Chem.* **2002**, *40*, 2719−2728.
(2) Lee, C. C.; MacKay, J. A.; Fréchet, J. M. J.; Szoka, F. C. *Nat. Biotechnol.* **2005**, 1517−1526.
(3) Twyman, L. J.; King, A. S. H.; Martin, I. K. *Chem. Soc. Rev.* **2002**, *31*, 69−82.
(4) Archut, A.; Azzellini, G. C.; Balzani, V.; Cola, L. D.; Vögtle, F. *J. Am. Chem. Soc.* **1998**, *120*, 12187−12191.
(5) Kojima, C.; Haba, Y.; Fukui, T.; Kono, K.; Takagishi, T. *Macromolecules* **2003**, *36*, 2183-2186.
(6) Kimura, M.; Kato, M.; Muto, T.; Hanabusa, K.; Shirai, H. *Macromolecules* **2000**, *33*, 1117−1119.
(7) Xu, J.; Luo, S.; Shi, W.; Liu, S. *Langmuir* **2006**, *22*, 989−997.
(8) Haba, Y.; Harada, A.; Takagishi, T.; Kono, K. *J. Am. Chem. Soc.* **2004**, *126*, 12760−12761.
(9) Suwa, K.; Morishita, K.; Kishida, A.; Akashi, M. *J. Polym. Sci., Part A: Polym. Chem.* **1997**, *35*, 3087−3094.
(10) Ito, S. *Koubunshi Ronbunsyu* **1989**, *46*, 437−443.
(11) Haba, Y.; Harada, A.; Takagishi, T.; Kono, K. *Polymer* **2005**, *46*, 1813−1820.
(12) Feil, H.; Bae, Y. H.; Feijen, J.; Kim, S. W. *Macromolecules* **1993**, *26*, 2496−2500.
(13) Broto, P.; Moreau, G.; Vandycke, C. *Eur. J. Med. Chem.* **1984**, *19*, 71−78.
(14) Schild, H. G.; Tirrell, D. A. *Langmuir* **1991**, *7*, 1319−1324.
(15) Hayashi, H.; Kono, K.; Takagishi, T. *Bioconjugate Chem.* **1999**, *10*, 412−418.
(16) Parrott, M. C.; Marchington, E. B.; Valliant, J. F.; Adronov, A. *J. Am. Chem. Soc.* **2005**, *127*, 12081−12089.
(17) Tono, Y.; Kojima, C.; Haba, Y.; Takahashi, T.; Harada, A.; Yagi, S.; Kono, K. *Langmuir* **2006**, *22*, 4920−4922.

MA061019A

Available online at www.sciencedirect.com

ScienceDirect

International Journal of Pharmaceutics 325 (2006) 186–190

INTERNATIONAL JOURNAL OF PHARMACEUTICS

www.elsevier.com/locate/ijpharm

Note

Enhancement of transfection activity of lipoplexes by complexation with transferrin-bearing fusogenic polymer-modified liposomes

Naoki Sakaguchi [a], Chie Kojima [a], Atsushi Harada [a], Kazunori Koiwai [b], Kazuhiro Shimizu [b], Nobuhiko Emi [c], Kenji Kono [a,*]

[a] *Department of Applied Chemistry, Graduate School of Engineering, Osaka Prefecture University, 1-1 Gakuen-cho, Nakaku, Sakai, Osaka 599-8531, Japan*
[b] *Research and Develop Center, Terumo Corporation, 1500 Inokuchi, Nakai-machi, Ashigarakamigun, Kanagawa 259-0151, Japan*
[c] *Department of Hematology, Fujita Health University School of Medicine, 1-98 Dengakugakubo, Kutsukake, Toyoake, Aichi 470-1192, Japan*

Received 9 October 2005; received in revised form 2 June 2006; accepted 8 June 2006
Available online 13 June 2006

Abstract

We previously developed complexes of lipoplexes containing 3β-(*N*-(*N'*,*N'*-dimethylaminoethane)carbamoyl)cholesterol (DC-chol) and succinylated poly(glycidol)-modified liposome, which becomes fusogenic under weakly acidic condition, for use as a novel gene delivery system. This study explored the effect of lipoplex structures – the type of cationic lipid and cationic lipid/DNA charge ratio – on the transfection activity of those complexes. Three types of cationic lipid with different polar groups were used for the preparation of lipoplexes: DC-chol, *N*-[1-(2,3-dioleoyloxy)propyl]-*N*,*N*,*N*-trimethylammonium methylsulfate (DOTAP), and 3,5-dipentadecyloxybenzamidine (TRX-20) with dimethylamino group, trimethylammonium group, and benzamidine group, respectively. Complexation with the SucPG-modified transferrin-bearing liposomes affected transfection activity of these lipoplexes differently. The TRX-20 lipoplexes exhibited the most marked enhancement of transfection activity upon complexation with the SucPG-modified liposomes among these lipoplexes. The cationic lipid/DNA charge ratio of the lipoplex and the amount of the transferrin-bearing SucPG-modified liposomes associated to the lipoplex also affected the transfection activity of the resultant complexes. Highly potent gene vectors were obtained by adjusting these factors.

Keywords: Gene delivery; Fusogenic liposome; Cationic liposome; Transferrin; Lipoplex

Numerous efforts have been made to develop efficient non-viral vectors for gene therapy (Brown et al., 2001; Niidome and Huang, 2002). Lipoplexes and polyplexes are respective complexes of cationic liposomes and cationic polymers with DNA. They are currently viewed as promising systems, but their activity can be improved. These systems bind to the cell surface through electrostatic interactions and are taken up by cells mainly via endocytosis. Subsequently, some parts of the gene contained in the complexes reach the nucleus, where gene transcription occurs. However, most of the complexes are likely to be trapped in the endosome, to be degraded eventually in the lysosome (Friend et al., 1996, Mönkkönen and Urtti, 1998). Therefore, to achieve efficient transfection of cells, gene vectors must possess an ability to promote gene transferral from the endosome to the cytosol before degradation in the lysosome (Zabner et al., 1995; Pouton and Seymour, 1998). Various methods have been used to enhance the endosomal escape of the entrapped gene, such as the use of membrane active molecules (Wagner, 1999, Kamata et al., 1994, Simoes et al., 1998, Kichler et al., 1997) and proton sponge effect (Sonawane et al., 2003; Boussif et al., 1995; Takahashi et al., 2003, 2005). Especially for lipoplexes, induction of fusion with endosome is one of the most efficient approaches to promote transfer of gene into cytosol and increase transfection efficiency (Farhood et al., 1995; Mok and Cullis, 1997).

In a previous study (Kono et al., 2001), we prepared complexes of lipoplexes and liposomes modified with transferrin-bearing succinylated poly(glycidol) (SucPG), which generate fusogenic activity at mildly acidic pH (Fig. 1) (Kono et al., 1994, 1997). These complexes, which are termed SucPG complexes, were designed to achieve cell transfection through efficient internalization into cells through transferrin receptor-mediated

* Corresponding author. Tel.: +81 722 54 9330; fax: +81 722 54 9330.
E-mail address: kono@chem.osakafu-u.ac.jp (K. Kono).

0378-5173/$ – see front matter © 2006 Elsevier B.V. All rights reserved.
doi:10.1016/j.ijpharm.2006.06.015

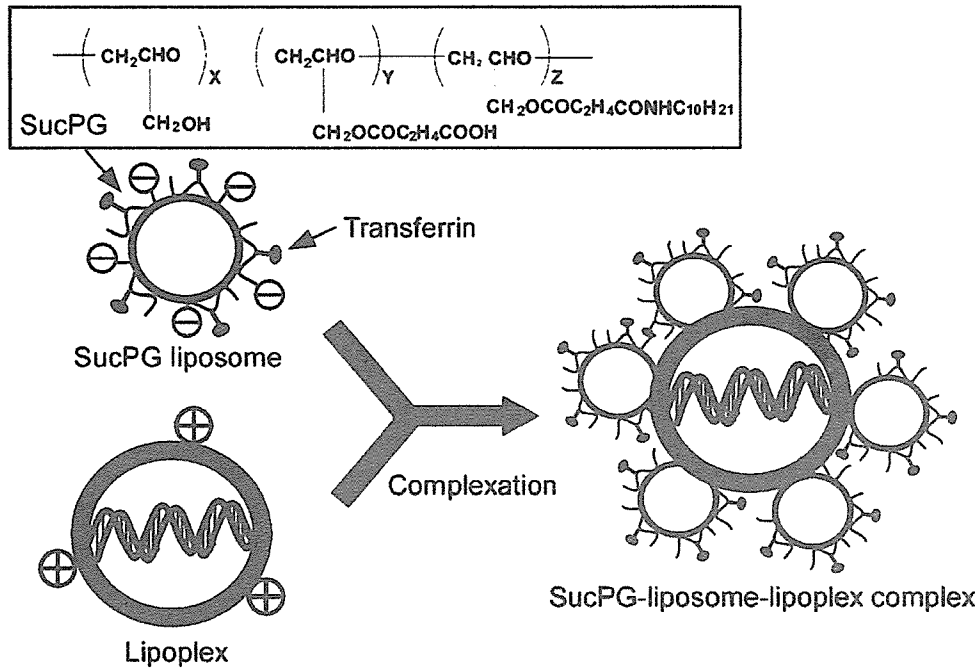

Fig. 1. Structure of SucPG having *n*-decyl groups and preparation of SucPG-complex bearing transferrin.

endocytosis and subsequent release of DNA into the cytoplasm by fusion with endosomal membrane. These complexes have a structure in which negatively charged SucPG-modified liposomes are associated with positively charged lipoplexes through electrostatic interaction. Transfection activity of DC-chol lipoplexes was actually enhanced by complexation with SucPG-modified liposomes. However, it remains unknown how the structure and properties of lipoplexes affect their transfection activity upon complexation with the SucPG-modified transferrin-bearing liposomes. To elucidate those questions, this study prepared lipoplexes from cationic lipids having different types of head groups: DC-chol with dimethylamino group, DOTAP with trimethylammonium group, and TRX-20 with benzamidine group (Fig. 2) (Harigai et al., 2001). Using them, we examined the effect of complexation of these lipoplexes with the transferrin-bearing SucPG liposomes on their transfection activity. Here, we report the influence of lipoplexes' structural properties – the type of cationic lipids and charges – on the fusogenic liposome-mediated enhancement of transfection activity of the lipoplexes.

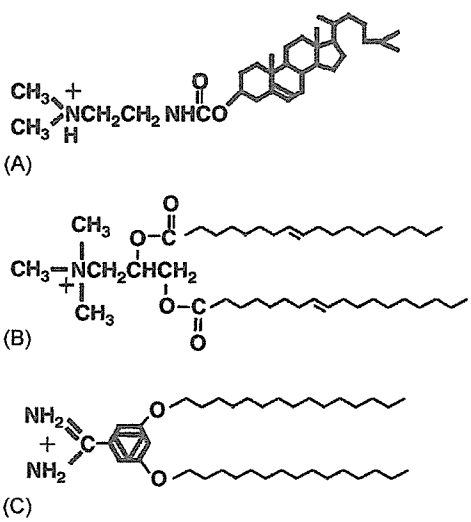

Fig. 2. Structures of DC-chol (A), DOTAP (B) and TRX-20 (C).

For the preparation of lipoplexes, cationic liposomes with three kinds of cationic lipids: DC-chol, DOTAP, and TRX-20 were used. These cationic liposomes contained phospholipids, such as DOPE and DLPC, in addition to cationic lipids. Compositions of these cationic liposomes were optimized to exhibit high transfection activity and determined as follows: DC-chol/DOPE (45:55, mol/mol); DOTAP/DOPE (1:1, mol/mol); TRX-20/DOPE/DLPC (1:2:1, mol/mol/mol).

Lipoplexes and SucPG complexes were prepared as reported previously (Kono et al., 2001). SucPG with the composition (x:y:z, Fig. 1) of 18:74:8 (mol/mol/mol) and the number-average molecular weight of 23,500 was used. These cationic liposomes were incubated with plasmid p10[18,23], which contains a firefly luciferase coding sequence derived from pGL3-basic (Promega) between Raus sarcoma virus LTR and polyadenylation signal in phosphate-buffered saline (PBS) for 10 min. Also, SucPG-modified liposomes were prepared by suspending a mixture of SucPG and egg yolk phosphatidylcholine in PBS and subsequent extrusion through a polycarbonate membrane with a pore size of 50 nm and conjugation of transferrin using 1-ethyl-3-(3-dimethylaminopropyl)carbodiimide as previously reported (Kono et al., 2001).

Table 1 lists the zeta potential and diameter of liposomes used in this study. The diameter of SucPG-modified liposomes was 65 nm, which was approximately the pore size of the polycarbonate membrane used for liposome extrusion. The zeta potential of the SucPG-modified liposomes indicates that these liposomes

Table 1
Diameter and zeta potential of liposomes

Liposome	Diameter (nm)	Zeta potential (mV)
TRX-20	146 ± 29	35.6 ± 3.5
DC-chol	201 ± 40	27.3 ± 2.3
DOTAP	141 ± 35	27.1 ± 2.4
SucPG	65 ± 13	−25.1 ± 2.9

Measurements were performed at 25 °C at pH 7.

possess negatively charged surfaces because of their negatively charged carboxylate groups on the SucPG chains. On the other hand, diameters and zeta potentials of these cationic liposomes were, respectively, between 140 and 200 nm and between 27 and 36 mV. Thus, irrespective of cationic lipid types, these liposomes possess similar sizes and surface charge densities.

The SucPG complexes were prepared by incubating the lipoplexes with varying amounts of the SucPG-modified liposome bearing transferrin for 5 min in an ice bath according to the method previously reported (Kono et al., 2001). Fig. 3A represents zeta potentials of various lipoplexes and their complexes with varying amounts of SucPG-modified liposomes. These lipoplexes exhibited zeta potentials around 20–27 mV. However, their zeta potentials decreased with increasing amount of SucPG-modified liposomes added to the lipoplexes, indicating that these lipoplexes formed complexes with SucPG-modified liposomes with similar efficiency. Their zeta potentials reached a constant value of about −20 mV at the succinylated unit/nucleotide unit ratio above 10, implying that the lipoplexes were covered with the SucPG-modified liposomes.

Diameters of the complexes of the lipoplexes–SucPG-modified liposomes were evaluated using dynamic light scattering (Fig. 3B). Their diameters changed depending on their composition and exhibited maximum at the succinylated unit/nucleotide unit ratio around four to seven, where the complexes became electrically neutral (Fig. 3A). Complex formation between the lipoplex and SucPG-modified liposomes was further confirmed from their morphology using atomic force microscopy. The TRX-20 lipoplex had a smooth surface, but a highly rough surface with many projections of about

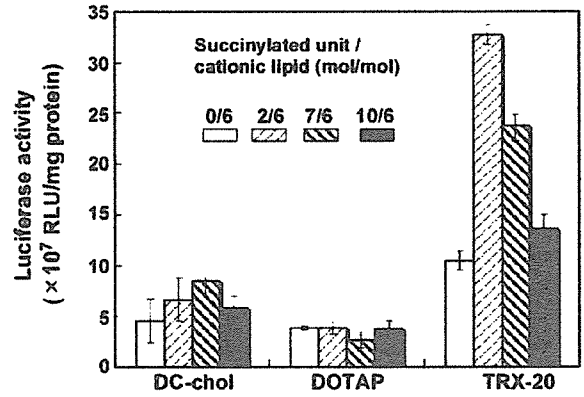

Fig. 4. Transfection activity of SucPG complexes prepared by incubating DC-chol, DOTAP and TRX-20 lipoplexes with varying amounts of SucPG-modified liposomes bearing transferrin. Luciferase activities of HeLa cells treated with SucPG complexes and their parent lipoplexes (open bars) are shown. The lipid/DNA (+/−) charge ratio of the lipoplexes was 6. The compositions of SucPG complexes are expressed as succinylated unit/cationic lipid (mol/mol) ratio in the figure. Each bar is the mean ± S.D. ($n = 3$). The cells (5×10^4) were treated with vectors containing 1 μg DNA in the presence of 10% FCS.

70–100 nm was observed after the complexation with SucPG-modified liposomes, suggesting that SucPG-modified liposomes were adsorbed onto the lipoplexes (results not shown).

The effect of complexation with SucPG-modified liposomes on transfection activity of these lipoplexes was examined. Fig. 4 presents expression of luciferase gene in HeLa cells treated with various complexes prepared by mixing, at varying ratios, lipoplexes of various types and the SucPG-modified transferrin-bearing liposomes. That figure shows that the effect of the fusogenic liposome complexation varies depending on the lipoplex type, even though these lipoplexes have equal cationic lipid/DNA phosphate (mol/mol) ratios. The transfection activity of the DOTAP lipoplex hardly changed, irrespective of the amount of the SucPG-modified liposomes mixed. In contrast, the TRX-20 lipoplex activity was markedly enhanced by addition of the fusogenic liposomes. The produced SucPG-complex exhibited a remarkably higher transfection activity than the parent TRX lipoplex when an appropriate amount of SucPG-modified

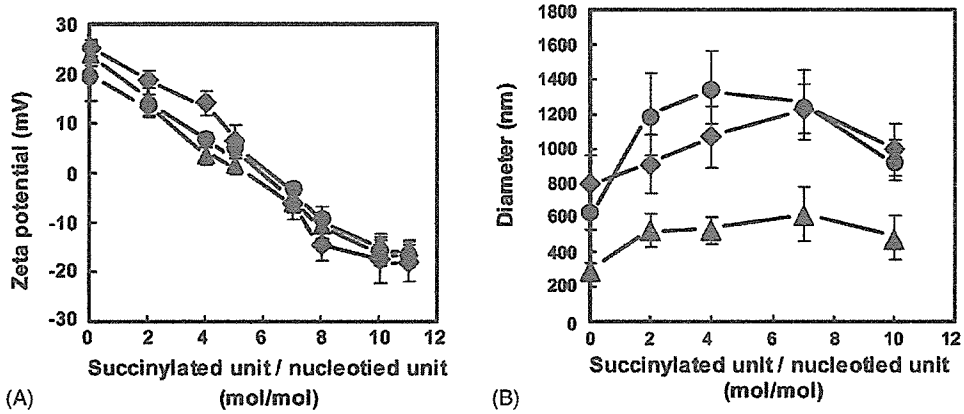

Fig. 3. Zeta potentials (A) and diameters (B) of SucPG-complexes prepared by incubating DC-chol (circles), DOTAP (triangles) and TRX-20 (diamonds) lipoplexes with varying amounts of SucPG-modified liposomes. The lipid/DNA (+/−) charge ratio of the lipoplexes was 6. The compositions of SucPG complexes are expressed as succinylated unit/DNA nucleotide unit ratio in the figure.

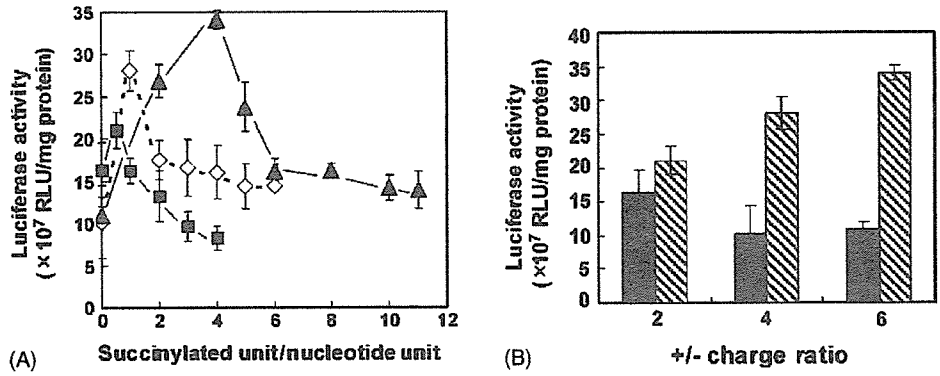

Fig. 5. Transfection activity of SucPG complexes prepared by complexation of TRX-20 lipoplexes and varying amounts of transferrin-bearing SucPG-modified liposomes. TRX-20 lipoplexes with the lipid/DNA (+/−) charge ratios of 2 (squares), 4 (diamonds), and 6 (triangles) were used as the starting lipoplexes. (A) Effect of composition on transfection activity of the complexes. The composition of the complex was expressed as the molar ratio of succinylated unit of SucPG-modified liposomes to DNA nucleotide units of the lipoplex. (B) Comparison of transfection activities between the SucPG complexes with optimum composition (hatched bars) and their parent lipoplexes (closed bars) with the lipid/DNA (+/−) charge ratios of 2, 4, and 6. Each point (A) or bar (B) is the mean ± S.D. ($n = 3$). The cells (5×10^4) were treated with vectors containing 1 μg DNA in the presence of 10% FCS.

liposomes was mixed to these lipoplexes. A similar tendency was shown for the DC-chol lipoplex. However, transfection activity of the DC-chol lipoplex was lower than that of the TRX-20 lipoplex and promotion of activity by complexation with the SucPG-modified liposomes was less marked than in the case of TRX-20 lipoplex.

Next we examined the influence of the cationic lipid/DNA (+/−) charge ratio of the TRX-20 lipoplexes on activity of the resultant SucPG-complexes because the TRX-20 lipoplex showed remarkable enhancement of transfection activity by complexation with SucPG-modified liposomes. The TRX-20 lipoplexes with the +/− charge ratios of 2, 4 and 6 were used for complexation with SucPG-modified liposomes. Fig. 5A shows that, irrespective of charge ratios, the transfection activity of the lipoplexes rose with increasing amount of the SucPG-modified liposomes added. However, complexation using too much SucPG-modified liposome degraded the activity. Fusion ability of the complexes increases concomitant with an increasing amount of the associated SucPG-modified liposomes, whereas the addition of too much SucPG-modified liposome might cause appearance of unassociated SucPG-modified liposome. These free SucPG-modified liposomes bear transferrin on the surface. Therefore, they might inhibit binding of the liposome–lipoplex complex to the cells because of interaction between the transferrin and its receptor. Consequently, appropriate amounts of the SucPG-modified liposomes were mixed with the lipoplexes to obtain maximum activity. The lipoplexes with charge ratios of 2, 4, and 6, respectively, produced SucPG complexes with maximum activity at the succinylated unit/phosphate unit ratios of 0.5, 1.0 and 4.0. Though the lipoplex with a high +/− charge ratio requires more SucPG-modified liposomes to achieve maximum activity, stronger activity is obtainable using lipoplexes with a higher +/− charge ratio.

Fig. 5B depicts transfection activities of the SucPG-complexes with the optimum composition and their parent lipoplexes. The SucPG complexes' activity increased remarkably with increasing +/− charge ratio of the lipoplexes used for their preparation. However, the activity of the parent lipoplexes tends to decrease concomitant with an increased charge ratio. This result indicates that activity of the SucPG complexes does not correlate with the activity of the parent lipoplex. The SucPG-complex made from the lipoplex with a high +/− charge ratio contained more SucPG-modified liposomes in the optimized composition. This complex might therefore have higher fusion ability and stronger affinity to the cell surface because of the transferrin–transferrin receptor interaction, implying stronger transfection activity.

This study has demonstrated that complexation of lipoplexes with the transferrin-bearing SucPG-modified liposomes is an effective method to obtain potent non-viral vectors that achieve gene transfection of cells through specific interaction between transferrin and its receptor. The effect of their complexation on transfection activity of the resultant complex depends on structural properties of lipoplex, such as the type of cationic lipid and the lipid/DNA charge ratio, and the amount of the SucPG-modified liposomes associated to the lipoplex. Because some complexes obtained by using TRX-20-based lipoplexes with appropriate charge ratios and the amount of the associated SucPG-modified liposomes achieved more efficient transfection of HeLa cells than widely used transfection reagents, such as DC-chol and DOTAP, these complexes are considered to be a promising candidate of non-viral vectors. In addition, complexation of the ligand-bearing SucPG-modified liposomes with other types of vectors may generate novel types of potent non-viral vectors.

References

Boussif, O., Lezoualc'h, F., Zanta, M.A., Mergny, M.D., Scherman, D., Demeneix, B., Behr, J.P., 1995. A versatile vector for gene and oligonucleotide transfer into cells in culture and in vivo: polyethylenimine. Proc. Natl. Acad. Sci. U.S.A. 92, 7297–7301.

Brown, M.D., Schätzlein, A.G., Uchegbu, I.F., 2001. Gene delivery with synthetic (non-viral) carriers. Int. J. Pharm. 229, 1–21.

Farhood, H., Serbina, N., Huang, L., 1995. The role of dioleoylphosphatidylethanolamine in cationic liposome mediated gene transfer. Biochim. Biophys. Acta 1235, 289–295.

Friend, D.S., Papahadjopoulos, D., Debs, R.J., 1996. Endocytosis and intracellular processing accompanying transfection mediated by cationic liposomes. Biochim. Biophys. Acta 1278, 41–50.

Harigai, T., Kondo, M., Isozaki, M., Kasukawa, H., Hagiwara, H., Uchiyama, H., Kimura, J., 2001. Preferential binding of polyethylene glycol-coated liposomes containing a novel cationic lipid, TRX-20, to human subendothelial cells via chondritin sulfate. Pharm. Res. 18, 1284–1290.

Kamata, H., Yagisawa, H., Takahashi, S., Hirata, H., 1994. Amphiphilic peptides enhance the efficiency of liposome-mediated DNA transfection. Nucleic Acids Res. 22, 536–537.

Kichler, A., Mechtler, K., Behr, J.P., Wagner, E., 1997. Influence of membrane-active peptides on lipospermine/DNA complex mediated gene transfer. Bioconjugate Chem. 8, 213–221.

Kono, K., Zenitani, K., Takagishi, T., 1994. Novel pH-sensitive liposomes: liposomes bearing a poly(ethylene glycol) derivatives. Biochim. Biophys. Acta 1193, 1–9.

Kono, K., Igawa, T., Takagishi, T., 1997. Cytoplasmic delivery mediated by liposomes modified with a pH-sensitive poly(ethylene glycol) derivative. Biochim. Biophys. Acta 1325, 143–154.

Kono, K., Torikoshi, Y., Mitsutomi, M., Itoh, T., Emi, N., Yanagie, H., Takagishi, T., 2001. Novel gene delivery systems: complexes of fusogenic polymer-modified liposomes and lipoplexes. Gene Ther. 8, 5–12.

Mok, K.W.C., Cullis, P.R., 1997. Structural and fusogenic properties of cationic liposomes in the presence of plasmid DNA. Biophys. J. 73, 2534–2545.

Mönkkönen, J., Urtti, A., 1998. Lipid fusion in oligonucleotide and gene delivery with cationic lipids. Adv Drug Delivery Rev. 34, 37–49.

Niidome, T., Huang, L., 2002. Gene therapy progress and prospects: non-viral vectors. Gene Ther. 9, 1647–1652.

Pouton, C.W., Seymour, L.W., 1998. Key issues in non-viral gene delivery. Adv. Drug Deliv. Rev. 34, 3–19.

Simoes, S., Slepushkin, V., Gaspar, R., de Lima, M.C.P., Düzgünes, N., 1998. Gene delivery by negatively charged ternary complexes of DNA, cationic liposomes and transferrin or fusogenic peptides. Gene Therapy 5, 955–964.

Sonawane, N.D., Szoka Jr., F.C., Verkman, A.S., 2003. Chloride accumulation and swelling in endosomes enhances DNA transfer by polyamine–DNA polyplexes. J. Biol. Chem. 278, 44826–44831.

Takahashi, T., Kono, K., Itoh, T., Emi, N., Takagishi, T., 2003. Synthesis of novel cationic lipids having polyamidoamine dendrons and their transfection activity. Bioconjugate Chem. 14, 764–773.

Takahashi, T., Harada, A., Emi, N., Kono, K., 2005. Preparation of efficient gene carriers using a polyamidoamine dendron-bearing lipid: improvement of serum resistance. Bioconjugate Chem. 16, 1160–1165.

Wagner, E., 1999. Application of membrane-active peptides for non-viral gene delivery. Adv. Drug Deliv. Rev. 38, 279–289.

Zabner, J., Fasbender, A.J., Moninger, T., Poellinger, K.A., Welsh, M.J., 1995. Cellular and molecular barriers to gene transfer by a cationic lipid. J. Biol. Chem. 270, 18997–19007.

International Journal of
HEMATOLOGY

Identification of Human Neutrophils during Experimentally Induced Inflammation in Mice with Transplanted CD34$^+$ Cells from Human Umbilical Cord Blood

Masaru Doshi, Makoto Koyanagi, Masako Nakahara, Koichi Saeki, Kumiko Saeki, Akira Yuo

Department of Hematology, Research Institute, International Medical Center of Japan, Tokyo, Japan

Received February 10, 2006; received in revised form June 1, 2006; accepted June 22, 2006

Abstract

Nonobese diabetic/severe combined immunodeficiency/γ chain^{null} (NOG) mice are excellent recipients for xenotransplantation and have been especially valuable for the evaluation of human hematopoietic stem cell (HSC) activities. Because human hematopoietic cells that developed in this mouse were mainly lymphoid cells and not myeloid cells, mature human myeloid cells such as neutrophils were hardly detectable in peripheral blood. We demonstrated that human neutrophils accumulated by means of a zymosan-induced air pouch inflammation technique could be identified with a fluorescence-activated cell sorter in NOG mice with transplanted CD34$^+$ cells from human umbilical cord blood, which were putative hematopoietic progenitor cells including HSC. Our results indicate that human neutrophils with a chemotactic capacity can develop from human hematopoietic progenitor cells in vivo, suggesting that our system may be a useful tool for the evaluation of human HSC activities.

Int J Hematol. 2006:84:231-237. doi: 10.1532/IJH97.06040

Key words: NOG mice; Transplantation; Human hematopoietic stem cells; Human neutrophils; Chemotaxis

1. Introduction

Hematopoietic stem cells (HSC) have been defined to possess both the ability to self-renew and the capacity to differentiate into full lineages of hematopoietic cells [1], capabilities that have been evaluated by the transplantation of human cells into experimental animals. Nonobese diabetic/severe combined immunodeficiency (NOD/SCID) mice have widely been used as recipients in xenotransplantation to evaluate the abilities of human HSC, although the engraftment rate of human hematopoietic cells in these mice has been low [2].

NOD/SCID/γ chain (γc)^{null} (NOG) mice, an NOD/SCID mouse strain that lacks the interleukin 2 receptor γc, were recently established to improve the engraftment efficiency of the conventional NOD/SCID mouse, which possesses natural killer cell activity [3]. Several studies have demonstrated that human hematopoietic cells develop in hematopoietic tissue or the peripheral blood of NOG mice that have received transplants of human hematopoietic progenitor cells, such as umbilical cord blood (CB) and bone marrow CD34$^+$ cells containing HSC [3-6]. However, because the human hematopoietic cells that developed in these mice were mainly lymphoid cells and not myeloid cells [4-6], mature human myeloid cells such as neutrophils were hardly detectable in the peripheral blood of the mice that had received such transplants. Therefore, no study has definitely identified human neutrophils in mice with transplanted human hematopoietic progenitor cells.

Human neutrophils, a primary constituent of peripheral blood leukocytes, play an important role during host defense against invading microorganisms [7]. The decreased numbers of neutrophils or attenuated function of neutrophils results in serious infections in several pathologic situations, such as congenital leukocyte function deficiencies or myelosuppression caused by chemotherapy [8,9]. The microbicidal functions of neutrophils are executed via total harmonization of all their specific functions, such as chemotaxis, adhesion, phagocytosis, and respiratory burst activity [10]. Several conventional methods are available to evaluate these effector functions of human neutrophils in vitro [11]. In addition, some functions, such as chemotaxis,

Correspondence and reprint requests: Akira Yuo, MD, PhD, Department of Hematology, Research Institute, International Medical Center of Japan, 1-21-1, Toyama, Shinjuku-ku, Tokyo 162-8655, Japan; 81-3-3202-7181; fax: 81-3-3207-1038 (e-mail: yuoakira@ri.imcj.go.jp).

can be evaluated in vivo by using the acute-inflammation model in mice [12].

Acute inflammation is induced by the injection of zymosan into a dorsal air pouch created in a mouse and the subsequent accumulation of a large number of murine neutrophils into the air pouch [13,14]. Consequently, highly purified murine neutrophils with a sufficient capacity to migrate from other sites, such as the peripheral blood, into inflammatory sites can be isolated from mice by means of this inflammation model. Our objective was to investigate whether the zymosan-injection air pouch methodology can be used in immunodeficient mice with transplanted human HSC to elicit neutrophil migration and inflammation. This methodology gives us the opportunity to evaluate not only human neutrophil production but also critical functions of engrafted human neutrophils.

2. Materials and Methods

2.1. Animals

The experimental protocol was approved by the Committee of Animal Care and Experiments of the Research Institute of the International Medical Center of Japan (IMCJ) (protocol no. 17-Tg-7). NOG mice were purchased from the Central Institute of Experimental Animals (CIEA) (Kanagawa, Japan). All mice were kept under specific pathogen-free conditions at the animal laboratory of the Research Institute of IMCJ in accordance with CIEA guidelines.

2.2. Transplantation of Human CB $CD34^+$ Cells into Mice

Nine-week-old female NOG mice were sublethally irradiated with 2 Gy via an MBR1520-3 x-ray source (Hitachi Medical, Tokyo, Japan). After 24 hours, mice received intravenous transplants of 1.8×10^5 human CB $CD34^+$ cells (AllCells, Berkeley, CA, USA) or vehicle (saline). The purity and viability of the CB $CD34^+$ cells were greater than 95%.

2.3. Zymosan-Induced Air Pouch Inflammation

Six, 8, or 10 weeks after the transplantation of human CB $CD34^+$ cells, a subcutaneous air pouch was formed on the back of NOG mice, as has been described previously [13,14]. Five hundred microliters of zymosan solution (1 mg/mL in saline) was injected into the air pouch. Sixteen hours after zymosan injection, mice were decapitated under diethyl ether anesthesia, and the air pouch was washed with 1 mL of ice-cold phosphate-buffered saline (PBS) to obtain accumulated leukocytes.

2.4. Determination of Superoxide Release

Superoxide release stimulated by phorbol myristate acetate was assayed by the superoxide dismutase–inhibitable reduction of ferricytochrome c, which was monitored continuously in a Hitachi 556 double-wavelength spectrophotometer (Hitachi High-Technologies, Tokyo, Japan) equipped with a thermostatted cuvette holder (37°C), as described previously [11].

2.5. Preparation of Neutrophils from Human Peripheral Blood

Granulocytes and mononuclear cells were prepared from healthy adult donors as described previously [11] by using dextran (Nacalai Tesque, Kyoto, Japan) sedimentation, centrifugation with a separating solution (Lymphoprep; Axis-Shield, Oslo, Norway), and hypotonic lysis of the contaminating erythrocytes. Neutrophils constituted greater than 90% of the granulocyte fractions, and the remaining cells were eosinophils. Mononuclear cell fractions consisted of 20% monocytes and 80% lymphocytes. Both cell fractions were suspended in PBS containing 5% fetal calf serum (FCS).

2.6. Preparation of Murine Bone Marrow and Spleen Leukocytes

Bone marrow cells were harvested from the mice by flushing the femurs with ice-cold Hanks balanced salt solution (HBSS). Spleens were harvested from the mice and minced in ice-cold HBSS. The resulting cell suspensions were filtered through a nylon mesh, and contaminating erythrocytes were eliminated by hypotonic lysis. The cells were then washed once and suspended in PBS containing 5% FCS.

2.7. Determination of Cell Surface Antigens by Fluorescence-Activated Cell Sorting

All suspensions of single cells were stained with the appropriate antibodies and analyzed by fluorescence-activated cell sorting (FACS) with a FACSCalibur flow cytometer (BD Biosciences, San Jose, CA, USA). Cells were incubated with monoclonal antibodies for 30 minutes on ice in PBS containing 5% FCS. Nonspecific binding to cells bearing Fcγ receptors was blocked with a rat antimouse CD16/CD32 monoclonal antibody (BD Biosciences). The following monoclonal antibodies were used in this flow cytometric study: fluorescein isothiocyanate (FITC)-conjugated rat antimouse Ly-6G and Ly-6C antibody (Gr-1 antibody) (BD Biosciences), phycoerythrin (PE)-conjugated mouse antihuman CD45 (BD Biosciences), PE-conjugated mouse antihuman CD10 (BD Biosciences), FITC-conjugated mouse antihuman CD66b (Beckman Coulter, Miami, FL, USA), and each isotype as a control. Antimouse Gr-1 antibody, which reacts selectively with murine neutrophils, does not cross-react with human hematopoietic cells, including neutrophils, and antihuman CD45, CD10, and CD66b antibodies, which react selectively with human neutrophils, do not cross-react with murine neutrophils.

2.8. Immunocytochemical Study

Cells collected from air pouches were washed with PBS and fixed on glass slides by means of a Cytospin apparatus (Cytospin 2; Shandon, Pittsburgh, PA, USA). After further fixation with acetone/methanol solution (1:3), immunostaining was performed as described previously [15] by using FITC-conjugated antihuman CD16b monoclonal antibody (Beckman Coulter) or antihuman CD45 monoclonal

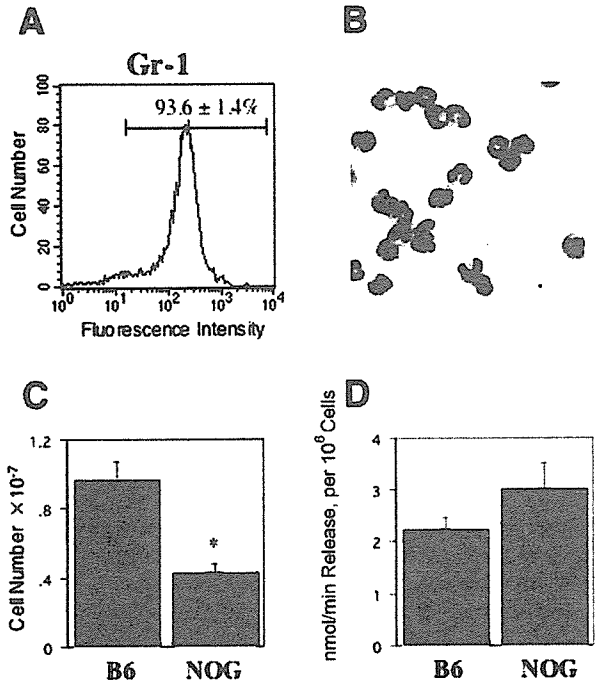

Figure 1. Air pouch inflammatory model in nonobese diabetic/severe combined immunodeficiency/γ chain^{null} (NOG) mice. Zymosan suspended in saline (0.5 mg/mouse) was injected into the air pouch of NOG mice to induce inflammation. The pouch was washed with phosphate-buffered saline 16 hours after zymosan injection to obtain accumulated leukocytes. A, Fluorescence-activated cell-sorting analysis of the expression of the granulocyte-specific antigen Gr-1 was carried out with leukocytes from the air pouch of NOG mice (n = 3). B, Morphology of the leukocytes in the air pouch of NOG mice. After fixation to glass slides, cells were stained with Wright-Giemsa solution and examined by light microscopy. C, The number of leukocytes in the air pouch was determined in B6 and NOG mice. D, The respiratory burst activities of granulocytes in the air pouch in B6 and NOG mice. Superoxide (O_2^-) release stimulated by 100 ng/mL phorbol myristate acetate was determined by the reduction of cytochrome *c* and is expressed as nmol/minute per 10^6 cells. Data for (C) and (D) are expressed as the mean ± SE (n = 6), and statistical analysis was performed by means of an unpaired Student *t* test. *$P < .05$, NOG versus B6 mice.

antibody (BD Biosciences). For the control, an isotype antibody reaction was performed by using FITC-conjugated immunoglobulin M (IgM) κ (ICN Biomedicals, Aurora, OH, USA) and IgG1 κ (BD Biosciences) for the anti-CD16b and anti-CD45 antibody reactions, respectively. The second antibody reaction was performed by using Alexa Fluor 488 goat antimouse IgM (Invitrogen, Carlsbad, CA, USA) and Alexa Fluor 488 goat antimouse IgG (Invitrogen) for the anti-CD16b and anti-CD45 antibody reactions, respectively.

2.9. Morphologic Observation

Cells were fixed on glass slides with a Cytospin 2 apparatus, stained with Wright-Giemsa solution (Muto Pure Chemical, Tokyo, Japan), and then observed with a light microscope (Olympus Optical, Tokyo, Japan).

2.10. Statistical Analysis

Statistical analysis was performed by means of the unpaired Student *t* test and the StatView software package (version 5.0; SAS Institute/Abacus Concepts, Berkeley, CA, USA).

3. Results

3.1. Zymosan-Induced Air Pouch Inflammation in NOG Mice

The leukocytes that accumulate by zymosan-induced air pouch inflammation in normal mice are known to be predominantly neutrophils, along with small numbers of monocytes and lymphocytes (data for normal B6 mice are not shown) [13,14]. In the present study, we first investigated whether zymosan-induced accumulation of mature murine neutrophils into the air pouch also occurs in NOG mice.

As has been observed with this inflammatory model in normal mice, the leukocytes that accumulated in the air pouch after zymosan injection in NOG mice were predominantly neutrophils. This result was established by detecting the expression of a specific surface antigen of mouse neutrophils, Gr-1, as well as the typical morphologic characteristics obtained via Wright-Giemsa staining (Figures 1A and 1B). Both the FACS analysis of the Gr-1 antigen and the morphologic evaluation indicated that greater than 90% of the accumulated leukocytes were neutrophils. In the NOG mice lacking lymphocytes, the remaining leukocytes (<10%) were monocytes (data not shown).

These results indicate that the migration of neutrophils toward inflammatory sites occurs almost normally in NOG mice, suggesting that the neutrophils of NOG mice have a normal chemotactic function. The number of leukocytes in the air pouch of NOG mice, however, was significantly lower ($P < .05$) than that of B6 mice (Figure 1C). On the other hand, the respiratory burst activity, another important function of neutrophils, was normal, because agonist-induced superoxide release from the leukocytes in the air pouch of NOG mice was equivalent to that of B6 mice (Figure 1D).

3.2. Engraftment of Human CB CD34$^+$ Cells in NOG Mice

We next transplanted human CB CD34$^+$ cells into recipient NOG mice. After being sublethally irradiated, NOG mice received intravenous transplants of human CB CD34$^+$ cells. Six weeks after transplantation, leukocytes in the bone marrow and spleen were analyzed for the expression of the human panleukocyte marker, CD45 (Figure 2). In these hematopoietic organs, approximately 90% of the cells expressed human CD45 antigen, both at 6 weeks and at 8 weeks after the transplantation of human CB CD34$^+$ cells (Figure 2). These findings indicate the highly effective engraftment of human hematopoietic cells in this immunodeficient mouse, and the efficiency of engraftment obtained in

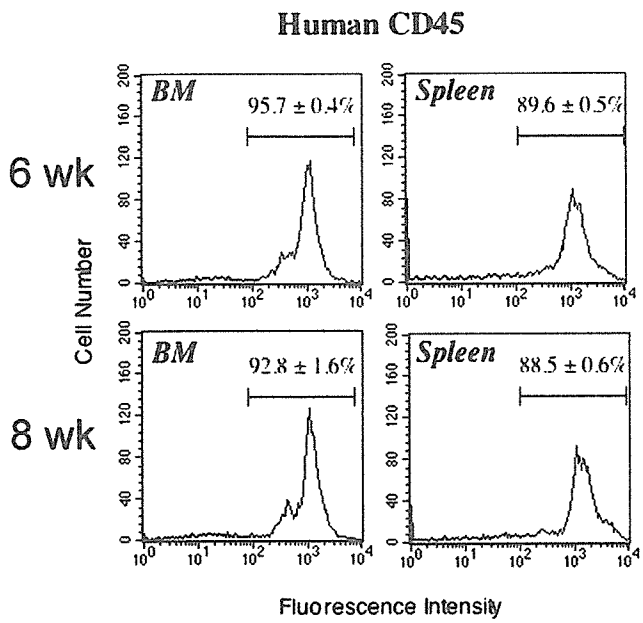

Figure 2. Engraftment of human cord blood CD34⁺ cells in nonobese diabetic/severe combined immunodeficiency/γ chain^{null} (NOG) mice. CD34⁺ cells from human umbilical cord blood (1.8×10^5 cells/mouse) were transplanted into NOG mice intravenously. Bone marrow (BM) and spleen leukocytes were obtained at 6 and 8 weeks after transplantation as described in "Materials and Methods." Cell surface expression of human CD45 was determined by fluorescence-activated cell-sorting analysis. Data are expressed as the mean ± SE (n = 3).

this study was equivalent to or better than the results described in previous reports [3,4].

We then evaluated whether CD45⁺ human hematopoietic cells appear in the air pouch of NOG mice that had received transplants of human CB CD34⁺ cells. As is shown in Figure 3 (upper panel), more than 90% of the leukocytes in the air pouch of NOG mice infused with vehicle alone were Gr-1⁺ murine neutrophils, and there were no human CD45⁺ leukocytes. In contrast, a significant level (approximately 10%) of human CD45⁺ cells in the air pouch was present in NOG mice that had received transplants of human CB CD34⁺ cells, and there was a concomitant decrease in the percentage of Gr-1⁺ murine neutrophils. We observed these findings at both 6 weeks and 8 weeks after transplantation of human CB CD34⁺ cells, although the human CD45⁺ cells in the air pouch had decreased at 8 weeks for an unknown reason.

3.3. Identification of Human Neutrophils Accumulated by Zymosan-Induced Air Pouch Inflammation in Mice with Transplanted Human CB CD34⁺ Cells

Because most of the leukocytes in zymosan-induced air pouch inflammation were neutrophils, the human CD45⁺ leukocytes in Figure 3 were considered human neutrophils that had differentiated in vivo in the NOG mice. To further confirm this hypothesis, we performed FACS analysis with monoclonal antibodies that specifically recognize mature human neutrophils. We selected 2 neutrophil-specific cell surface molecules, CD10 and CD66b. CD10, well known as a common acute lymphoblastic leukemia antigen [16], has been reported to be expressed in mature neutrophils [17-19], and CD66b is a specific cell surface antigen of human granulocytes [20].

Before the transplantation experiments with NOG mice, we performed several experiments with normal human neutrophils and mononuclear leukocytes to establish experimental conditions for the 2-color flow cytometric analysis of CD10 and CD66b. As is shown in Figure 4 (upper panel), we successfully performed 2-color analysis with a granulocyte fraction isolated from a healthy donor. The granulocyte fraction contained 96.5% CD66b⁺ granulocytes, which consisted of 86.3% CD10⁺ neutrophils and 10.2% other CD10⁻ granulocytes, probably eosinophils. This granulocyte fraction contained more than 98% CD45⁺ cells (data not shown). In contrast, the cells in mononuclear cell fractions were negative for both CD66b and CD10.

Using this analytical condition, we then performed a 2-color flow cytometric analysis of the leukocytes that had

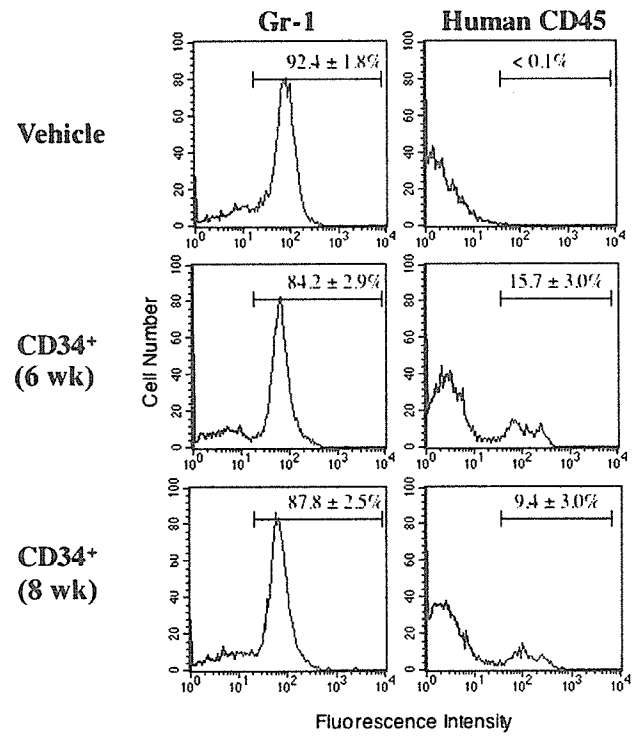

Figure 3. Identification of human leukocytes in the air pouch of nonobese diabetic/severe combined immunodeficiency/γ chain^{null} (NOG) mice. CD34⁺ cells from human umbilical cord blood (1.8×10^5 cells/mouse) (CD34⁺) or saline (vehicle) was transplanted into NOG mice intravenously. Zymosan was suspended in saline (0.5 mg/mouse) and injected into the air pouch to induce inflammation by 6 or 8 weeks after transplantation. The pouch was washed with phosphate-buffered saline 16 hours after zymosan injection to obtain accumulated leukocytes. Cell surface expression of murine Gr-1 and human CD45 was determined by fluorescence-activated cell-sorting analysis. Data are expressed as the mean ± SE (n = 3).

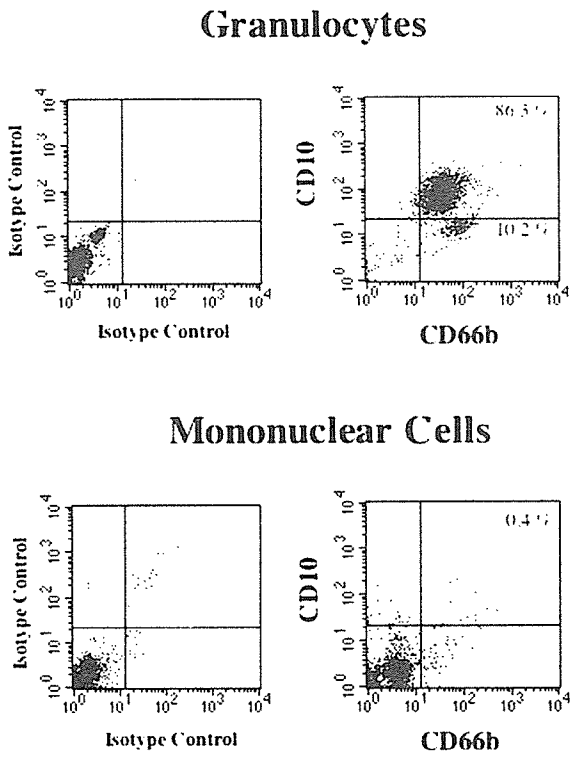

Figure 4. Two-color fluorescence-activated cell-sorting (FACS) analysis of CD10 and CD66b in human peripheral blood leukocytes. Human granulocytes and mononuclear cells were isolated as described in "Materials and Methods." Two-color FACS analysis of the cell surface expression of human CD10 and CD66b was performed with each isotype antibody as a control.

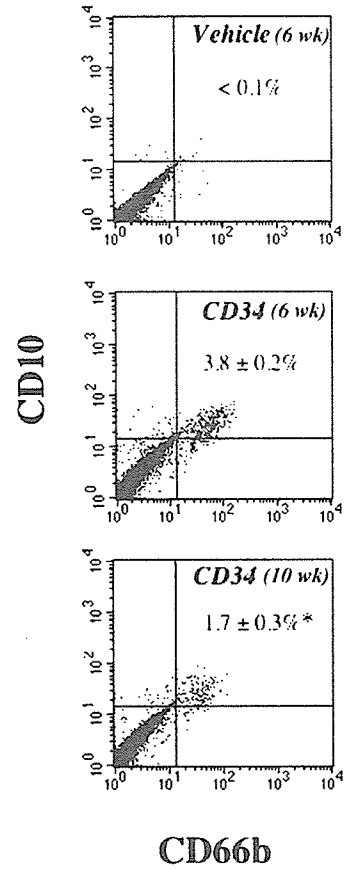

Figure 5. Two-color fluorescence-activated cell-sorting (FACS) analysis of CD10 and CD66b in leukocytes in the zymosan-induced air pouch in nonobese diabetic/severe combined immunodeficiency/γ chain^{null} (NOG) mice with transplanted human umbilical cord blood (CB) CD34$^+$ cells. Human CB CD34$^+$ cells (1.8×10^5 cells/mouse) were transplanted into NOG mice intravenously. Zymosan suspended in saline (0.5 mg/mouse) was injected into the air pouch to induce inflammation at 6 or 10 weeks after transplantation (middle and lower panels). Sixteen hours after zymosan injection, the pouch was washed with phosphate-buffered saline to obtain accumulated leukocytes. Cell surface expression of human CD10 and CD66b was determined by FACS analysis. As a negative control, leukocytes that had accumulated in the air pouch in NOG mice without CD34$^+$ cell transplantation were analyzed, and the results are shown in the top panel. Data are expressed as the mean ± SE (n = 3). Statistical analysis was performed by means of an unpaired Student *t* test. *$P < .05$, 10 weeks versus 6 weeks.

accumulated in the air pouch after zymosan injection into mice with transplanted human CB CD34$^+$ cells. As is shown in Figure 5, double-positive (both CD10$^+$ and CD66b$^+$) human neutrophils were detected in the air pouch at both 6 weeks and 10 weeks after the transplantation of human CB CD34$^+$ cells. It is interesting that the double-positive human neutrophils in the air pouch had decreased by 10 weeks, compared with the numbers at 6 weeks. These data for double-positive human neutrophils in the air pouch almost corresponded to the data estimated from the numbers of human CD45$^+$ leukocytes in the air pouch (data not shown).

Finally, we used immunocytochemical staining to confirm that human neutrophils actually existed in the air pouch following zymosan injection into mice with transplanted human CB CD34$^+$ cells. As is shown in Figure 6, we were able to detect human CD45$^+$ cells with a neutrophil morphology in the leukocytes that had accumulated in the air pouch of mice with transplanted human CB CD34$^+$ cells. In contrast, human CD45$^+$ cells were not observed in the leukocytes that had accumulated in the air pouch of mice that had not undergone transplantation (data not shown). The presence of human neutrophils in the air pouch of mice with transplanted human CB CD34$^+$ cells was also confirmed with antihuman neutrophil-specific CD16b antibody (Figure 7).

Thus, using an in vivo inflammatory model, we have shown the functional engraftment of human neutrophils.

4. Discussion

Mature human neutrophils derived from human hematopoietic progenitor cells have not been identified in the peripheral blood of immunodeficient mice with transplanted human HSC, although HSC are considered to dif-

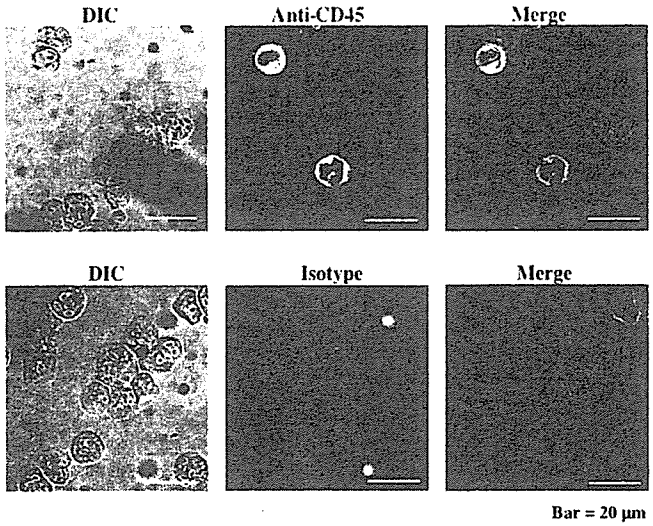

Figure 6. Immunocytochemical analysis of CD45 in leukocytes in the zymosan-induced air pouch in nonobese diabetic/severe combined immunodeficiency/γ chain^{null} (NOG) mice with transplanted CD34$^+$ cells from human umbilical cord blood (CB). Human CB CD34$^+$ cells (1.8×10^5 cells/mouse) were transplanted into NOG mice intravenously. Zymosan suspended in saline (0.5 mg/mouse) was injected into the air pouch to induce inflammation at 6 weeks after transplantation. The pouch was washed with phosphate-buffered saline 16 hours after zymosan injection to obtain accumulated leukocytes. Immunocytochemical analysis of human CD45 expression (top) was performed with isotype antibody as a control (bottom), and the staining pattern was observed with an inverted microscope. The left panels are difference interference contrast (DIC) images, the middle panels are the corresponding images obtained by fluorescence microscopy, and the right panels are combined images of the corresponding left and middle panels.

ferentiate into all hematopoietic cell lineages, including neutrophils. In the present study, we established a novel system to detect human neutrophils in NOG mice with transplanted human CB CD34$^+$ cells by using a model of experimentally induced inflammation and a 2-color FACS analysis that used 2 monoclonal antibodies specific for mature human neutrophils and/or granulocytes (Figure 5). In addition, the results obtained with our system, which selectively detects neutrophils that have migrated into the site of inflammation, indicated that the functional human neutrophils had developed from human hematopoietic progenitor cells in vivo.

Analysis of the cell surface antigens of leukocytes by FACS has been widely performed in many immunologic and hematologic studies because morphologic identification has not been capable of distinguishing lymphocyte subpopulations. In contrast, studies for specific cell surface markers of human neutrophils have been extremely limited, because human neutrophils are easily recognized by their morphology and there are no distinct subpopulations with the same morphology. However, to distinguish precisely between human and mouse neutrophils in chimeric mice with transplanted human hematopoietic progenitor cells requires determining specific cell surface antigens of human neutrophils. In the murine system, Gr-1 is a well-known granulocyte-specific cell surface marker and is known as a common epitope of Ly-6 subtypes in mice [21]. Stroncek et al reported that CD177, known as human neutrophil-specific antigen NB1, was a member of the Ly-6 gene superfamily and that it might be a human counterpart of Gr-1 [22]. However, the level of CD177 expression in human neutrophils is approximately 50% (unpublished data), suggesting that CD177 is not suitable for the complete identification of human neutrophils. In contrast, the present study clearly revealed that human neutrophils could be identified by a 2-color FACS analysis of 2 cell surface antigens, CD10 and CD66b, which are specific markers for granulocytes and/or neutrophils (Figure 4).

We found that neutrophil accumulation during zymosan-induced acute inflammation was reduced in NOG mice, compared with B6 mice (Figure 1C). Zymosan is known to activate the alternative pathway of complement and C5a formation [12], and inflammatory mediators, such as arachidonate metabolites, that are released from resident macrophages upon zymosan stimulation cause neutrophils to accumulate at the site of inflammation [23]. NOG mice have multiple immunologic defects in innate immunity, including a lack of macrophage function, complement-dependent hemolytic activity, and natural killer cell activity [3]. Therefore, the reduction of macrophage function and complement-

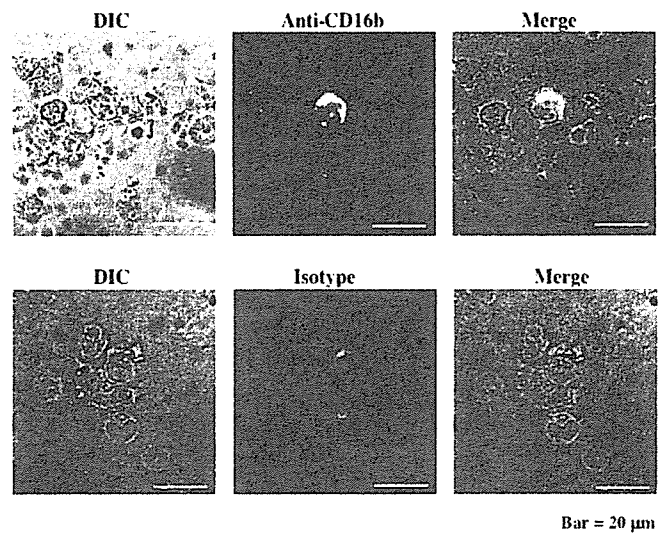

Figure 7. Immunocytochemical analysis of CD16b in leukocytes in the zymosan-induced air pouch in nonobese diabetic/severe combined immunodeficiency/γ chain^{null} (NOG) mice with transplanted CD34$^+$ cells from human umbilical cord blood (CB). Human CB CD34$^+$ cells (1.8×10^5 cells/mouse) were transplanted into NOG mice intravenously. Zymosan suspended in saline (0.5 mg/mouse) was injected into the air pouch to induce inflammation at 6 weeks after transplantation. The pouch was washed with phosphate-buffered saline 16 hours after zymosan injection to obtain accumulated leukocytes. Immunocytochemical analysis of human CD16b expression (top) was performed with isotype antibody as a control (bottom), and the staining pattern was observed with an inverted microscope. The left panels are difference interference contrast (DIC) images, the middle panels are the corresponding images obtained by fluorescence microscopy, and the right panels are combined images of the corresponding left and middle panels.

dependent hemolytic activity may account for the reduction of neutrophil accumulation during zymosan-induced acute inflammation in NOG mice. On the other hand, superoxide-producing capacity, another important function of neutrophils, was normal in NOG mice (Figure 1D). Therefore, the development and function of neutrophils are considered normal to some degree in NOG mice.

Previous studies have shown that engraftment of human $CD45^+$ cells in NOG mice is lymphocyte predominant and that engraftment increases gradually for 4 to 12 weeks following the transplantation of human CB $CD34^+$ cells [3,5,6]. On the other hand, we found that the engraftment of human neutrophils as estimated by our in vivo air pouch inflammatory model declined from 6 to 10 weeks after the transplantation of human $CD34^+$ cells (Figures 3 and 5). Although the exact reason for these different observations remains unclear, there are 2 possibilities: (1) extremely different life cycle and production kinetics for neutrophils and lymphocytes, or (2) the relatively normal development of murine neutrophils versus an almost complete lack of murine lymphocytes in NOG mice.

Investigators have recently concluded that human embryonic stem cells constitute a valuable resource for regenerative medicine because of their high capacity to differentiate into a broad range of cell types [24]. Consequently, many researchers have been vigorously studying such cells to establish culture conditions and techniques for the in vitro differentiation of human embryonic stem cells into hematopoietic stem or progenitor cells [25,26]. For clinical applications, however, both the differentiation and therapeutic potential of such cells should be investigated and evaluated in vivo, although performing such in vivo studies is not allowed in human beings. Therefore, our system may be useful as an in vivo system to evaluate the hematopoietic activities, particularly granulopoietic, of human hematopoietic progenitor cells derived from human embryonic stem cells.

Acknowledgment

This work was supported by a Sasakawa Scientific Research Grant from the Japan Science Society.

References

1. Osawa M, Hanada K, Hamada H, Nakauchi H. Long-term lymphohematopoietic reconstitution by a single CD34-low/negative hematopoietic stem cell. *Science.* 1996;273:242-245.
2. Greiner DL, Hesselton RA, Shultz LD. SCID mouse models of human stem cell engraftment. *Stem Cells.* 1998;16:166-177.
3. Ito M, Hiramatsu H, Kobayashi K, et al. NOD/SCID/γc^{null} mice: an excellent recipient mouse model for engraftment of human cells. *Blood.* 2002;100:3175-3182.
4. Matsumura T, Kametani Y, Ando K, et al. Functional $CD5^+$ B cells develop predominantly in the spleen of NOD/SCID/γc^{null} (NOG) mice transplanted either with human umbilical cord blood, bone marrow, or mobilized peripheral blood $CD34^+$ cells. *Exp Hematol.* 2003;31:789-797.
5. Kambe N, Hiramatsu H, Shimonaka M, et al. Development of both human connective tissue-type and mucosal-type mast cells in mice from hematopoietic stem cells with identical distribution pattern to human body. *Blood.* 2004;103:860-867.
6. Yahata T, Ando K, Nakamura Y, et al. Functional human T lymphocyte development from cord blood $CD34^+$ cells in nonobese diabetic/Shi-*scid*, IL-2 receptor γ null mice. *J Immunol.* 2002;169:204-209.
7. Witko-Sarsat V, Rieu P, Descamps-Latscha B, Lesavre P, Halbwachs-Mecarelli L. Neutrophils: molecules, functions and pathophysiological aspects. *Lab Invest.* 2002;80:617-653.
8. Johnston RB Jr. Clinical aspects of chronic granulomatous disease. *Curr Opin Hematol.* 2001;8:17-22.
9. Johnston EM, Crawford J. Hematopoietic growth factors in the reduction of chemotherapeutic toxicity. *Semin Oncol.* 1998;25:552-561.
10. Yuo A. Differentiation, apoptosis, and function of human immature and mature myeloid cells: intracellular signaling mechanism. *Int J Hematol.* 2001;73:438-452.
11. Yuo A, Kitagawa S, Ohsaka A, et al. Recombinant human granulocyte colony-stimulating factor as an activator of human granulocytes: potentiation of responses triggered by receptor-mediated agonists and stimulation of C3bi receptor expression and adherence. *Blood.* 1989;74:2144-2149.
12. Rao TS, Currie JL, Shaffer AF, Isakson PC. In vivo characterization of zymosan-induced mouse peritoneal inflammation. *J Pharmacol Exp Ther.* 1994;293:917-925.
13. Posadas I, Terencio MC, Guilltén I, Ferrándiz ML, Payá M, Alcaraz MJ. Co-regulation between cyclo-oxygenase-2 and inducible nitric oxide synthase expression in the time-course of murine inflammation. *Naunyn Schmiedebergs Arch Pharmacol.* 2000;361:98-106.
14. Doshi M, Watanabe S, Niimoto T, et al. Effect of dietary enrichment with n-3 polyunsaturated fatty acids (PUFA) or n-9 PUFA on arachidonate metabolism *in vivo* and experimentally induced inflammation in mice. *Biol Pharm Bull.* 2004;27:319-323.
15. Saeki K, Yasugi E, Okuma E, et al. Proteomic analysis on insulin signaling in human hematopoietic cells: identification of CLIC1 and SRp20 as novel downstream effectors of insulin. *Am J Physiol Endocrinol Metab.* 2005;289:E419-E428.
16. Uckun FM, Ledbetter JA. Immunobiologic differences between normal and leukemic human B-cell precursors. *Proc Natl Acad Sci U S A.* 1988;85:8603-8607.
17. Braun MP, Martin PJ, Ledbetter JA, Hansen JA. Granulocytes and cultured human fibroblasts express common acute lymphoblastic leukemia-associated antigens. *Blood.* 1983;61:718-725.
18. Cossman J, Neckers LM, Leonard WJ, Greene WC. Polymorphonuclear neutrophils express the common acute lymphoblastic leukemia antigen. *J Exp Med.* 1983;157:1064-1069.
19. Iwamoto I, Kimura A, Ochiai K, Yoshida S. Distribution of neutral endopeptidase activity in human blood leukocytes. *J Leukoc Biol.* 1991;49:116-125.
20. Zhao L, Xu S, Fjaertoft G, Pauksen K, Hakansson L, Venge P. An enzyme-linked immunosorbent assay for human carcinoembryonic antigen-related cell adhesion molecule 8, a biological marker of granulocyte activities in vivo. *J Immunol Methods.* 2004;293:207-214.
21. Fleming TJ, Fleming ML, Malek TR. Selective expression of Ly-6G on myeloid lineage cells in mouse bone marrow: RB6-8C5 mAb to granulocyte-differentiation antigen (Gr-1) detects members of the Ly-6 family. *J Immunol.* 1993;151:2399-2408.
22. Stroncek DF, Caruccio L, Bettinotti M. *CD177*: a member of the Ly-6 gene superfamily involved with neutrophil proliferation and polycythemia vera. *J Transl Med.* 2004;2:8.
23. Lefkowith JB. Essential fatty acid deficiency inhibits the in vivo generation of leukotriene B4 and suppresses levels of resident and elicited leukocytes in acute inflammation. *J Immunol.* 1988;140:228-233.
24. Thomson JA, Itskovitz-Eldor J, Shapiro SS, et al. Embryonic stem cell lines derived from human blastocyst. *Science.* 1998;282:1145-1147.
25. Vodyanik MA, Bork JA, Thomson JA, Slukvin II. Human embryonic stem cell-derived $CD34^+$ cells: efficient production in the co-culture with OP9 stromal cells and analysis of lymphohematopoietic potential. *Blood.* 2006;105:617-626.
26. Wang L, Li L, Shojaei F, et al. Endothelial and hematopoietic cell fate of human embryonic stem cells originates from primitive endothelium with hemangioblastic properties. *Immunity.* 2004;21:31-41.

Blockade of bulky lymphoma-associated CD55 expression by RNA interference overcomes resistance to complement-dependent cytotoxicity with rituximab

Yasuhito Terui,[1,2] Takuma Sakurai,[1,3] Yuko Mishima,[1] Yuji Mishima,[2] Natsuhiko Sugimura,[2] Chino Sasaoka,[2] Kiyotsugu Kojima,[2] Masahiro Yokoyama,[1] Nobuyuki Mizunuma,[1] Shunji Takahashi,[1] Yoshinori Ito[1] and Kiyohiko Hatake[1,2,4]

[1]Division of Clinical Chemotherapy, and [2]Olympus Bio-Imaging Laboratory, Cancer Chemotherapy Center, Japanese Foundation for Cancer Research, Tokyo 135-8550, and [3]Material Research Laboratory, Morinaga Milk Industry, Zama, Kanagawa 228-8583, Japan

(Received August 29, 2005/Revised October 4, 2005/Accepted October 17, 2005/Online publication December 18, 2005)

Recently, anti-CD20 (rituximab) and anti-Her2/neu (trastuzumab) antibodies have been developed and applied to the treatment of malignant lymphoma and breast cancer, respectively. However, bulky lymphoma is known to be resistant to rituximab therapy, and this needs to be overcome. Fresh lymphoma cells were collected from 30 patients with non-Hodgkin's lymphoma, the expression of CD20 and CD55 was examined by flow cytometry, and complement-dependent cytotoxicity (CDC) assays were carried out. Susceptibility to CDC with rituximab was decreased in a tumor size-dependent manner ($r = -0.895$, $P < 0.0001$), but not in a CD20-dependent manner ($r = -0.076$, $P = 0.6807$) using clinical samples. One complement-inhibitory protein, CD55, contributed to bulky lymphoma-related resistance to CDC with rituximab. A decrease in susceptibility to CDC with rituximab was statistically dependent on CD55 expression ($r = -0.927$, $P < 0.0001$) and the relationship between tumor size and CD55 expression showed a significant positive correlation ($r = 0.921$, $P < 0.0001$) using clinical samples. To overcome the resistance to rituximab by high expression of CD55 in bulky lymphoma masses, small interfering RNA (siRNA) was designed from the DNA sequence corresponding to nucleic acids 1–380 of the CD55 cDNA. Introduction of this siRNA decreased CD55 expression in the breast cancer cell line SK-BR3 and in CD20-positive cells of patients with recurrent lymphoma; resistance to CDC was also inhibited. This observation gives us a novel strategy to suppress bulky disease-related resistance to monoclonal antibody treatment. (*Cancer Sci* 2006; 97: 72–79)

In recent years, monoclonal antibodies have been used increasingly to treat patients with malignancies such as lymphoma and breast cancer.[1–3] In particular, the anti-CD20 antibody, also called rituximab, is usually very effective for treatment of malignant lymphoma, and most patients can receive rituximab as monotherapy or combination chemotherapy.[4,5] However, in some cases with bulky mass and at stage IV, lymphoma cells become resistant to rituximab treatment.[6,7] Apart from the number of tumor cells being greater in these cases, how this resistance occurs has not yet been clarified.

Recently, some researchers have reported four mechanisms for the action of rituximab: (i) inhibition of proliferation; (ii) induction of apoptosis; (iii) complement-dependent cytotoxicity (CDC); and (iv) antibody-dependent cellular cytotoxicity (ADCC).[7,8] Because CDC could more rapidly and efficiently act on the target cells attacked by rituximab, CDC may be the most important of the mechanisms of rituximab.

The role of complementary regulatory proteins in the modulation of rituximab efficacy has been addressed, and several surface membrane proteins regulate the deposition of active complement proteins on cellular membranes to prevent cell lysis. Regulators of the complement system play an important role in CDC, and CD46, CD55 and CD59 are well known to inhibit the complement system.[9] Among these inhibitors, CD55 and CD59 seem to be the most important.[10] No differences in the expression of CD59 molecules have been reported between normal B cells and malignant B cells, whereas CD55 expression was shown to be different among individual patients with B-cell malignancy.[11] Nevertheless, *in vitro* susceptibility to rituximab-induced CDC could not be predicted by the level of these proteins in chronic lymphocytic leukemia (CLL) cells, and *in vivo* susceptibility could not be predicted in follicular lymphoma (FL) and CLL patients.[12,13] In contrast, some researchers have reported direct correlations among CDC, CD55 and CD59 using B-cell lines.[14]

CD55, also known as decay accelerating factor, is a major regulator of the alternative and classical pathways of complement activation and is expressed on all serum-exposed cells. CD55 is a 70-kDa glycoprotein, which is a glycosylphosphatidylinositol (GPI)-anchored protein.[15] CD55 can bind the complex of C3a and Bb, which is in the classical pathway, and it blocks the cascade of the complement system. A functional disorder of CD55 in blood cells causes paroxysmal nocturnal hemoglobinuria (PNH).[16] In these cases, the cascade of the complement system can not be controlled, and CDC activity is enhanced mainly against red blood cells. CD55 can enhance dissociation between C3 convertase and C4bC2/C3bBb complexes, and then inhibit the cascade of the

[4]To whom correspondence should be addressed. E-mail: khatake@jfcr.or.jp.

doi: 10.1111/j.1349-7006.2006.00139.x

complement system. While it is true that CD55 levels are low to absent in PNH, the disease is caused by phosphatidylinositol glycan-A (PIGA) gene mutations that lead to a failure to assemble GPI anchors. Hence, all GPI-anchored proteins are missing in this disease.

Previous researchers have shown that certain conditions for cancer cells, such as hypoxia, poor nutrition and bulky mass, make them chemoresistant.[17,18] When gastric cancer cells were exposed to hypoxia, hypoxia inducible factor (HIF)-1 was induced and the cells were resistant to Cis-platin (CDDP).[18] When lymphoid cells were able to resist doxorubicin (adriamycin), expression of nuclear factor (NF)-κB and its transcription activity were enhanced in doxorubicin (adriamycin)-resistant cells.[17]

Because CDC activity is especially important for rituximab therapy and CD55 may function as a mostly important inhibitor of CDC, it is possible that a decline in CDC activity by CD55 molecules may cause resistance to rituximab. CDC correlates directly with the expression of CD20 antigen in malignant B cells, and *in vitro* susceptibility to rituximab-mediated CDC depends primarily on CD20 protein expression. However, there have yet been no reports about the relationship between tumor size and sensitivity to CDC or between tumor size and CD55 expression.

More recently, small interfering RNA (siRNA) has been developed and applied to knock down target gene expression.[19] For example, the nuclear factor of activated T cells (NFAT) and NF-κB were shown to be constitutively active in large B-cell lymphoma cells, and downregulation of NFATc1 and NF-κB in malignant B-cell lymphoma with siRNA inhibited lymphoma cell growth.[20] Although many researchers tried siRNA for genes of membrane proteins such as growth factor receptors,[21] there have been no successful reports describing siRNA for complement inhibitors.

To clarify the resistance to rituximab and overcome the resistance, especially with regard to bulky mass unresponsiveness and efficacy for re-treatment, we examined the relationship between CDC activity and rituximab, and CD55 expression in our patients, using siRNA for CD55 to treat CDC with rituximab.

Materials and Methods

Cell lines

Human malignant B-cell lines as well as Daudi and Raji cells (ATCC) were cultured in RPMI-1640 (Gibco, Carlsbad, CA, USA) with 10% fetal calf serum (FCS) at 37°C. The cell lines were used as sensitive and resistant controls in CDC with anti-CD20 antibody. The human breast cancer cell lines MCF7 and SK-BR3 (ATCC) were cultured in Dulbecco's minimal essential medium (DMEM; Gibco) with 10% FCS.

Complement-mediated cytotoxicity assay

Cells were washed once with fresh complete medium, and anti-CD20 antibody (rituximab; Roche, Basel, Switzerland) or anti-Her2/neu antibody (trastuzumab; Roche) was added at a concentration of 20 μg/mL. Cells were incubated at 37°C for 1 h, and then human AB blood serum from healthy volunteers with informed consent was added at 20% (v/v). After incubation at 37°C for 1 h, propidium iodide (PI; Sigma, St Louis, MO, USA) was added and CDC assays were carried out by flow cytometry with FACscan (Becton Dickinson, San Jose, CA, USA). For CDC assays using a microplate reader, Daudi, Raji and SKBR3 cells were seeded at 1×10^5 cell/mL in each well, and then rituximab or trastuzumab (20 μg/mL) and normal AB serum (20% [v/v]) were added. The reaction was incubated at 37°C for 1 h, and the cells were washed with phosphate-buffered saline (PBS) at least three times. Ten microliters of Calcein-AM (2 μg/mL) (Dojindo, Kumamoto, Japan) was added to each well and mixed thoroughly. After incubation at room temperature, fluorescence intensity was measured at 485 nm/535 nm wavelengths with a microplate reader (Fluoroskan Ascent; Labsystems, Helsinki, Finland).

Surface markers

Cells were washed once with PBS, and were then were stained with phycoerythrin (PE)-conjugated anti-CD20, and fluoresceinisothiocyanate (FITC)-conjugated anti-CD55 (Becton Dickinson). Flow cytometry was then carried out using FACscan. The intensities of C20 and CD55 expression were normalized compared with a control. For confocal laser scanning microscopy, rituximab and trastuzumab were labeled with Alexa Fluor 594 (Molecular Probes; Invitrogen, Carlsbad, CA, USA) in accordance with the manufacturer's instructions. In brief, 100 μg of antibody was labeled with Alexa Fluor 594 for 20 min after alkalization with carbonate. The mixture was put into a spin column and spun down at 1500*g*, and the flow-through was collected as Alexa Fluor 594-conjugated antibody.

Laser scanning confocal microscopy and phase-contrast microscopy

To see CDC activity on living cells, pictures were taken by a CDC camera with phase-contrast microscopy after the CDC assay with rituximab or trastuzumab. The cells were also stained with Alexa Fluor 594-labeled rituximab or Alexa Fluor 594-labeled trastuzumab and FITC-labeled anti-CD55 antibody, and serum was added to the culture medium. The stained cells were observed in real time under a confocal laser scanning microscopy system (Olympus, Tokyo, Japan).

Collection of clinical samples

Fresh lymphoma cells were collected from the lymph nodes of 30 patients with non-Hodgkin's lymphoma (11 cases of diffuse large B-cell type, 10 cases of marginal zone cell type, five cases of follicular cell type, two cases of small lymphocytic type, one case of B-cell immunoblastic type, and one case of diffuse small cell type) after receiving informed consent. In brief, the lymph nodes were resected surgically and specimens were broken into small pieces with scissors and ground between two glass slides. The cells were collected after centrifugation and washed with RPMI-1640 containing 10% FCS. Cell counting and viability were assessed by toluidine-blue exclusion dye test, and CD19-positive cells were isolated using a magnetic cell sorting (MACS) system. The isolated cells were stained with FITC-conjugated anti-CD19, PE-conjugated anti-CD20, and FITC-conjugated anti-CD55 antibodies and flow cytometry was then carried out.